MEASUREMENTS OF THE LINEAR POLARIZATION OF RADIO SOURCES AT DECIMETER WAVELENGTHS

Thesis by

George Andrew Seielstad

In Partial Fulfillment of the Requirements

For the Degree of

Doctor of Philosophy

California Institute of Technology

Pasadena, California

1963

ACKNOWLEDGMENTS

I wish to thank G. J. Stanley, Observatory Director, for his generous allotment of uninterrupted observing time. Assistance with the observations was provided by G. L. Berge, R. W. Wilson, D. Morris, and V. Radhakrishnan, to all of whom I express my gratitude. J. F. Bartlett wrote a necessary computer program. Invaluable advice and criticism were provided by many, in particular D. Morris and V. Radhakrishnan. I am perhaps most deeply indebted to W. A. Munger, without whose encouragement I would never have seen this project to completion.

The research at the Owens Valley Radio Observatory is supported by the U. S. Office of Naval Research under Contract Nonr 220(19).

ABSTRACT

Measurements at three frequencies of the degree and preferred orientation of the linearly polarized radiation from twenty-five unresolved radio sources are reported. The frequencies used were 2840 Mc/s, 1666 Mc/s, and 1420 Mc/s. The results are combined with those of other observers in order to derive properties of the emitting sources and of the Galaxy. An interferometric technique for determining the distribution of polarized radiation within a radio source is developed and applied to a few sources. Calculations on some model source distributions are included.

TABLE OF CONTENTS

CHAPTER I

Introduction

As early as 1950, Alfvén and Herlofson (1) suggested the possibility that the radiating mechanism in the so-called "radio stars" was "synchrotron" emission from ultrarelativistic electrons moving in a magnetic field. It has been shown that the radiation from such a system of electrons when moving in a constant uniform magnetic field should be strongly linearly polarized (2), (3), (4). Of course, irregularities in the field reduce the expected degree of polarization. Consequently, the detection of linear polarization in the radiation from discrete radio sources would be strong support for the synchrotron theory, as well as an indication of highly ordered magnetic fields within the emitting sources.

Shklovsky (5) employed the synchrotron theory to explain the continuous radiation of the Crab Nebula. The discovery of a high degree of linear polarization in the optical radiation was reported shortly thereafter (6), (7), (8). Later, this object was found to be linearly polarized at centimeter and decimeter wavelengths as well (references 9 through 16).

Early attempts to detect linear polarization in the radio-frequency radiation from intense extragalactic sources were unsuccessful (10), (11), (15), (17), (18). However, the recent discovery by Mayer, McCullough, and Sloanaker (19)

of strongly polarized 3.15-cm radiation from Cygnus A resulted in intensified efforts at various observatories to detect polarization in extragalactic radio sources.

The present investigation reports on measurements of the degree and preferred orientation of linearly polarized radiation from discrete radio sources made with the two 90-foot antennas at the Owens Valley Radio Observatory operating as an interference polarimeter. Interferometric measurements require different techniques from the more familiar single-antenna method. The measurement technique and results for the unresolved sources are discussed in Chapter II; for the resolved sources, the discussion appears in Chapter IV. An Appendix contains calculations of visibility functions for various model sources of use in the latter discussion.

Observations were made at three frequencies. An analysis of the data can yield information about the physical conditions in our Galaxy, as well as in the emitting sources. This analysis is treated in Chapter III.

CHAPTER II

Observational Technique and Results for Unresolved Sources

The application of radio interferometric techniques to the study of discrete sources of radiation has been described in detail by Moffet (20). The assumption was made that the feed horns mounted at the focus of each antenna were linearly polarized and were oriented parallel to each other. Modification of his results is required to treat the case of an arbitrary feed-horn orientation. The necessary modification is developed here.

Interferometer Response to a Discrete Source of Radiation

It has been shown (20) that the monochromatic response pattern of a two-element, continuous-multiplication interferometer (21) is given by

$$R(x,y,t) = GA(x,y)\cos\left\{2\pi[s_x(x-\Omega t)+s_y y] + \Psi\right\} \qquad (1)$$

in a Cartesian coordinate frame (x,y) centered at the point (α_o, δ_o) on the celestial sphere. For $|x|<<1$ and $|y|<<1$, the transformation is

$$x = (\alpha-\alpha_o)\cos\delta_o = \left[\Omega\,(t-t_o)-(h-h_o)\right]\cos\delta_o\,, \quad y=\delta-\delta_o, \qquad (2)$$

Ω being the sidereal rate, t the sidereal time, h the hour angle, and δ the declination. In equation 1, s_x and s_y are the x- and y-components, respectively, of the antenna

separation in wavelengths s. G is the receiver gain, Ψ an instrumental phase error, and A(x,y) the effective area of either antenna, assumed identical. We shall ignore the effects of receiver bandwidth and concentrate on this monochromatic response.

Equation (1) was derived on the assumption that the signals incident on each antenna had the same phase but for the difference in path length, $\left[s_x(x-\Omega t)+s_y y\right]$, between the source and the two antennas. This assumption is valid only when the feed horns of each antenna are parallel. For an arbitrary feed-horn orientation, if we let ψ_k represent the instantaneous phase of the signal emitted in position angle p_k, there will be an additional phase difference $(\psi_k - \psi_1)$ between the signals reaching the two antennas. In general, then, the interferometer response pattern when one feed-horn is in position angle p_k and the other in p_1 is

$$R_{k1}(x,y,t) = GA(x,y)\cos\left\{2\pi\left[s_x(x-\Omega t)+s_y y\right]+\psi_k-\psi_1+\Psi\right\}. \quad (3)$$

Let us now consider the effect of a discrete source of radiation passing through the sensitivity pattern of the interferometer. Let the point (x,y) in the source emit radiation which, at a particular instant, in position angle p_k has a phase $\psi_k(x,y)$ and an amplitude of electric vibration $E_k(x,y)$. With the feed horns positioned as shown in Figure 1, the response of the interferometer to the source is the integral over the source distribution of the product of the

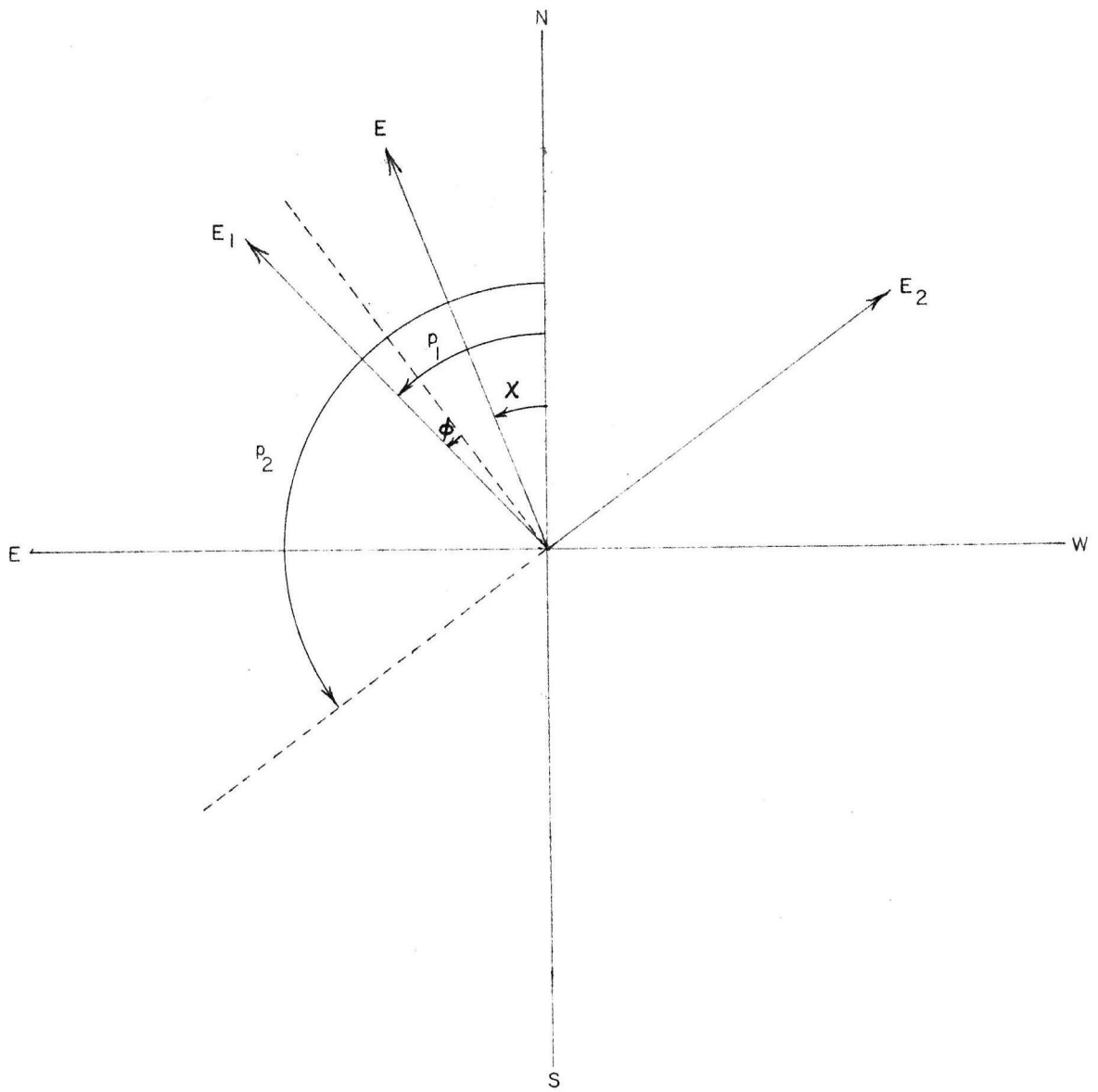

Figure 1. Orientation of feed horns. $\vec{E}_1$ is the E-plane of one linearly polarized feed, and $\vec{E}_2$ of the other. $\vec{E}$ is the plane of polarization of an incident linearly polarized electromagnetic wave. All position angles are measured from north toward east, modulo 180°.

sensitivity pattern of equation (3) and the voltages induced in each antenna:

$$R_{12}(t) = \langle G\iint A(x,y)E_1(x,y)E_2(x,y)$$
$$\cos\left\{2\pi\left[s_x(x-\Omega t)+s_y y\right]+\psi_1(x,y)-\psi_2(x,y)+\Psi\right\}dx\ dy\rangle$$
$$= G\iint A(x,y)\langle E_1(x,y)E_2(x,y)\cos\left[\psi_1(x,y)-\psi_2(x,y)\right]\rangle$$
$$\cos\left\{2\pi\left[s_x(x-\Omega t)+s_y y\right]+\Psi\right\}\ dx\ dy \qquad (4)$$
$$-G\iint A(x,y)\langle E_1(x,y)E_2(x,y)\sin\left[\psi_1(s,y)-\psi_2(x,y)\right]\rangle$$
$$\sin\left\{2\pi\left[s_x(x-\Omega t)+s_y y\right]+\Psi\right\}\ dxdy\ .$$

The brackets indicate a time average over an interval which is long compared to the period of the electromagnetic oscillations.

We now introduce the following definitions:

$$C_{12}(x,y) = \langle E_1(x,y)E_2(x,y)\cos\left[\psi_1(x,y)-\psi_2(x,y)\right]\rangle, \qquad (5)$$

$$S_{12}(x,y) = \langle E_1(x,y)E_2(x,y)\sin\left[\psi_1(x,y)-\psi_2(x,y)\right]\rangle. \qquad (6)$$

Then equation (4) can be put in the form

$$R_{12}(t) = G\left\{V_{12}(s_x,s_y)\cos\left[\Phi_{12}(s_x,s_y)-2\pi s_x\Omega t+\Psi\right]\right.$$
$$\left.-\Gamma_{12}(s_x,s_y)\sin\left[\sigma_{12}(s_x,s_y)-2\pi s_x\Omega t+\Psi\right]\right\}\ , \qquad (7)$$

where (V,Φ) and (Γ,σ) define the following complex Fourier transforms:

$$V_{12}(s_x,s_y)e^{i\Phi_{12}(s_x,s_y)}=\iint A(x,y)C_{12}(s,y)e^{i2\pi(s_x x+s_y y)}dx\ dy\ , \qquad (8)$$

$$\Gamma_{12}(s_x,s_y)e^{i\sigma_{12}(s_x,s_y)}=\iint A(x,y)S_{12}(x,y)e^{i2\pi(s_xx+s_yy)}dx\,dy. \tag{9}$$

Unresolved Linearly Polarized Sources

Considerable simplification results if we restrict the discussion to linearly polarized sources whose dimensions are much smaller than the fringe period $1/s$ of the interferometer. In this case the Fourier transforms defined by equations (8) and (9) assume their values at the point $(s_x=0,s_y=0)$, and the interferometer response becomes simply

$$R_{12}(t)=G\left[V_{12}(0,0)\cos(-2\pi s_x\Omega t+\Psi)-\Gamma_{12}(0,0)\sin(-2\pi s_x\Omega t+\Psi)\right]. \tag{10}$$

Let the source consist of a linearly polarized component, represented by the electric vector $\vec{E}$ in position angle χ, and an unpolarized component $\vec{U}$ (see Figure 1). The quantities C_{12} and S_{12} are easily evaluated if we employ the defining properties of unpolarized radiation. Products of any polarized component with any unpolarized component average to zero. Furthermore, the phases of orthogonal components of unpolarized radiation are uncorrelated; orthogonal components of linearly polarized radiation are either in phase or in antiphase. Consequently, we have

$$C_{12} = -\langle E^2\rangle\cos(p_1-\chi)\cos(p_2-\chi)-1/2\,\langle U^2\rangle\cos(p_2-p_1) \tag{11}$$

$$= -1/2\left\{\left[\langle E^2\rangle+\langle U^2\rangle\right]\cos(p_2-p_1)+\langle E^2\rangle\cos(p_1+p_2-2\chi)\right\}$$

and $$S_{12} = 0\ . \tag{12}$$

The Fourier transform of C_{12} is obtained by integrating over the source dimensions, which in the case of an unresolved source are sufficiently small that we can approximate as follows:

$$V_{12}(0,0) = \iint A(x,y)C_{12}(x,y)dx\,dy \approx A(0,0)C_{12}(0,0)\Delta x\,\Delta y\ .$$

If we denote by I_p and I_u the fluxes of the polarized and unpolarized components respectively, we find for the interferometer response to an unresolved linearly polarized source

$$R_{12}(t) = -(1/2)G\left[(I_p+I_u)\cos(p_2-p_1)+I_p\cos(p_1+p_2-2\chi)\right]$$

$$\cos(-2\pi s_x \Omega\, t+\Psi)\ . \qquad (13)$$

The response $R_{12}(t)$ is zero when

$$\cot(p_2-p_1) = -\frac{I_p\sin 2(p_2-\chi)}{I_p+I_u+I_p\cos 2(p_2-\chi)}\ . \qquad (14)$$

The polarization fraction m is defined by

$$m = \frac{I_p}{I_p + I_u}\ . \qquad (15)$$

If we let P_1 be the position angle of feed horn 1 for which, for a given position p_2 of feed horn 2, the interferometer response is zero, then equation (14) can be rewritten

$$\cot(p_2-P_1) = \tan\phi = -\frac{m\sin 2(p_2-\chi)}{1+m\cos 2(p_2-\chi)}\ , \qquad (16)$$

where we have introduced the angle ϕ defined by

$$\phi = \frac{\pi}{2} - (p_2 - P_1) \quad . \tag{17}$$

From equation (16) it is seen that the angle ϕ is zero when

$$p_2 = \chi + n\pi/2 \quad . \tag{18}$$

In addition, the function $\phi(p_2)$ has a maximum when its derivative vanishes, namely when

$$\cos 2(p_2 - \chi) = -m \tag{19}$$

and

$$\sin 2(p_2 - \chi) = \mp\sqrt{1-m^2} \quad . \tag{20}$$

When equations (19) and (20) are substituted into equation (16) to find the maximum value for the function $\phi(p_2)$, we obtain

$$\phi_{max} = \tan^{-1}\left[\cot 2(p_2 - \chi)\right] \quad .$$

Hence $2(p_2 - \chi) = \frac{3\pi}{2} - \phi_{max}$, and

$$m = \sin \phi_{max} \quad . \tag{21}$$

Observational Procedure and Analysis

The observing procedure is now obvious. Feed horn 2 is set at a series of fixed angles p_2 . For each such position, feed horn 1 is rotated until the angle P_1 is found which minimizes the interferometer response. Ideally, this

minimum is zero. In practice, however, many factors contribute to produce a residual signal, termed "instrumental polarization". Some of the contributing factors are the following: the feed horns may not be perfectly linearly polarized; the surfaces of the reflectors may not be truly parabolic, so that the antenna response pattern is not circularly symmetric about its axis; due to pointing errors the source may be observed off the axis of the main beam; the horn axis may be skewed relative to the reflector's axis, so that rotation of the horn produces a wobble of the beam; etc. Moreover, we expect the magnitude of these effects to vary as the position of the reflector is varied. Consequently, we must calibrate the system as a function of declination by observing several sources assumed to be unpolarized. The calibrating sources were selected from among Cassiopeia A, Cygnus A, Virgo A, Orion A, M 17, Hydra A, and CTB 31. The variation of the instrumental polarization with hour angle can be minimized by confining all observations to within one hour of meridian transit.

Having thus determined the angle P_1 for a number of calibrating sources of varying declinations, we can, using equation (17), plot a curve of ϕ_{cal} as a function of declination for each fixed value of p_2. For any source which we wish to study, the angles $(\phi - \phi_{cal})$ should fit the curve described by equation (16). The polarization fraction m is then given by equation (21), and the position angle χ of the E-vector of the polarized radiation is determined from

equation (18).

In all cases studied, the polarization fraction m was found to be an order of magnitude less than unity. To first order in this quantity equation (16) can be approximated by

$$\phi - \phi_{cal} \approx -m\sin 2(p_2-\chi), \qquad (22)$$

where the angle $(\phi - \phi_{cal})$ is expressed in radians. Thus, the experimentally determined values of $(\phi - \phi_{cal})$ were fitted by a least-squares analysis to a sinusoid, whose amplitude in radians was the polarization fraction m and whose positive-going crossover at position angle P_2 determined the polarization angle χ through the relation $\chi=P_2-\pi/2$.

Figure 2 shows examples of the fitting procedure to (a) 3C-286, (b) the Crab Nebula, and (c) 3C-295, all at a frequency of 2840 Mc/s and at an antenna separation of 290λ.

Results

The results obtained for the unresolved sources are presented in Table 1. A source is considered to be unresolved if its visibility amplitude, as determined by Moffet (20), is no less than 0.8. Observations were made at three frequencies: 2840 Mc/s, 1666 Mc/s, and 1420 Mc/s. The antennas were oriented on an east-west baseline with a physical separation of 200 feet. An additional set of measurements was made at 2840 Mc/s with an antenna separation of 100 feet. The separations listed in Table 1 are in units of wavelengths.

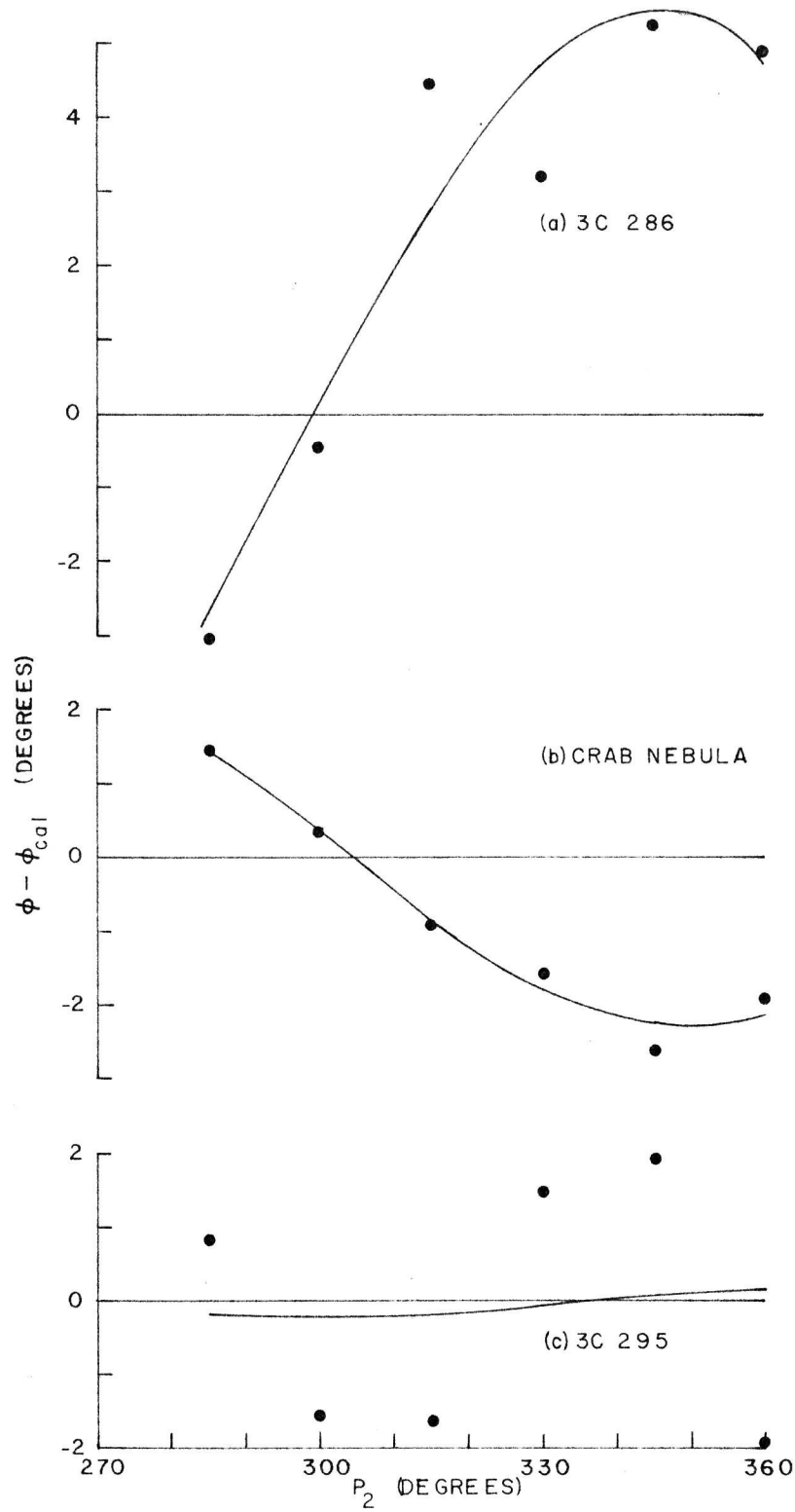

Figure 2. Fit of a sinusoid (solid curve) to the observed data (small circles) for (a) 3C-286, (b) the Crab Nebula, and (c) 3C-295.

Table 1. Polarization Fraction and Position Angle of E-Vector for Unresolved Sources

Frequency	2840 Mc/s				1666 Mc/s		1420 Mc/s	
Antenna Sep. (Wavelengths)	290λ		580λ		340λ		290λ	
Source	Pol. Fraction	Pos. Angle	Pol. Fraction	Pos. Angle	Pol. Fraction	Pos. Angle	Pol. Fraction	Pos. Angle
3C-20							1.8%±1.0%	126°±13°
3C-33	8.0%±1.3%	88°± 7°	4.9%±1.8%	96°±10°	7.2%±0.4%	72°± 2°	7.7 ±0.7	62 ± 3
3C-48			3.4 ±1.0	75 ±10			0.7 ±0.6	162 ±25
3C-78	2.3 ±1.7	85 ±14						
NGC 1275	1.5 ±1.0	102 ± 6	2.8 ±2.2	125 ±22	1.0 ±0.7	172 ±20	0.8 ±0.6	37 ±21
3C-98	7.0 ±2.8	111 ±11			5.8 ±0.4	16 ± 2	4.6 ±1.0	62 ± 6
3C-111	3.3 ±1.8	116 ±14			2.1 ±0.2	120 ± 5	2.2 ±0.6	92 ± 9
3C-123			0.4 ±0.3	69 ±15			0.5 ±0.4	68 ±24
Crab Nebula	3.9 ±0.2	124 ± 5			1.8 ±0.1	94 ± 2	1.6 ±0.4	85 ± 7
3C-147	0.9 ±0.9	104 ±18	0.7 ±1.2	58 ±46			0.2 ±0.5	138 ±57
3C-161	6.1 ±0.6	161 ± 5	9.5 ±1.2	168 ± 5	9.0 ±0.5	132 ± 2	5.9 ±0.5	29 ± 3
3C-196	1.8 ±1.2	85 ±11	1.0 ±1.3	95 ±34			0.4 ±0.5	155 ±38
3C-227	3.9 ±2.0	153 ±16						
M 82	3.5 ±1.3	35 ±11						

Table 1 (continued)

Frequency	2840 Mc/s				1666 Mc/s		1420 Mc/s	
Antenna Sep. (Wavelengths)	290λ		580λ		340λ		290λ	
Source	Pol. Fraction	Pos. Angle	Pol. Fraction	Pos. Angle	Pol. Fraction	Pos. Angle	Pol. Fraction	Pos. Angle
3C-273	3.4%±0.3%	147°± 4°			2.4%±0.3%	178°± 4°	1.9%±0.4%	171°± 6°
3C-286	9.5 ±1.2	30 ± 5	8.5%±1.1%	28°± 4°	8.7 ±0.5	34 ± 2	9.3 ±0.5	32 ± 2
3C-295	0.4 ±2.0	72 ±156					0.5 ±0.5	160 ±27
3C-327							3.7 ±1.6	7 ±14
Hercules A	6.3 ±0.9	31 ± 7			2.1 ±0.1	52 ± 2	1.4 ±0.4	59 ± 8
3C-353[1]	6.7 ±0.6	114 ± 5			3.8 ±0.3	165 ± 2	2.9 ±0.4	0 ± 4
SN 1604	0.8 ±0.9	117 ±34						
3C-380	1.0 ±0.8	21 ±24			1.6 ±0.3	34 ± 6	1.4 ±0.7	72 ±14
3C-433	5.4 ±1.2	121 ± 7	6.3 ±2.3	123 ±10	6.9 ±0.9	26 ± 4	4.7 ±0.6	150 ± 4
3C-444							0.9 ±0.7	169 ±23
Venus	0.6 ±1.1	111 ±54						

[1] Visibility amplitude is 0.75 at 290λ and 0.7 at 340λ.

The polarization fraction is defined by equation (15) and has been tabulated in per cent. The tabulated position angles refer to the E-vector of the polarized radiation, and are measured east from north, modulo 180°. The errors are standard deviations.

For all measurements, both sidebands of the superheterodyne receiver were accepted. The intermediate frequency was 10 Mc/s, and the bandwidths were each 5 Mc/s. Hatanaka (22) has demonstrated that one effect of a finite receiver bandwidth on a completely polarized signal which has passed through a magneto-ionic medium is to reduce the measured polarization fraction. His calculation was made on the assumption of a single-sideband receiver. We shall perform an analogous calculation for a double-sideband receiver.

For simplicity we assume that the receiver has two equal bandpasses, one bounded by the frequencies f_1 and f_2 and the other by f_3 and f_4. We represent the Stokes parameters characterizing the radiation in the infinitesimal frequency interval f to f+df by Idf, Qdf, Udf, and Vdf. For linearly polarized radiation these parameters have the values (see e.g. Cohen (23))

$$Qdf = I_p \cos 2\chi \, df, \tag{23}$$

$$Udf = I_p \sin 2\chi \, df, \tag{24}$$

$$Vdf = 0 , \tag{25}$$

where $I_p df$ is the intensity of polarized radiation in the interval df centered on f, and χ is the position angle at the frequency f of the plane of polarization. If the partially polarized signal has passed through a magneto-ionic medium, due to Faraday rotation the angle χ will vary inversely as the square of the frequency (see equation (35)):

$$\chi - \chi_o = A/f^2 \quad . \tag{26}$$

Here χ_o is the initial polarization angle, and A is a constant independent of frequency. Then

$$df = - \frac{f^3}{2A} d\chi \quad . \tag{27}$$

Radiation of different frequencies is, of course, incoherent. Therefore, the Stokes parameters $\overline{I}$, $\overline{Q}$, $\overline{U}$, and $\overline{V}$ for the total radiation accepted by the receiver are found by integrating equations (23) through (25) over the bandpass of the receiver. We assume that the frequency interval f_1 to f_4 is sufficiently small that I and I_p remain constant throughout. If we denote by χ_i the polarization angle corresponding to the frequency f_i, we have

$$\overline{I} = I\left[(f_2-f_1)+(f_4-f_3)\right] , \tag{28}$$

$$\overline{Q} = - \frac{f^3 I_p}{4A} \left[(\sin 2\chi_2-\sin 2\chi_1)+(\sin 2\chi_4-\sin 2\chi_3)\right] , \tag{29}$$

$$\overline{U} = - \frac{f^3 I_p}{4A} \left[(\cos 2\chi_1-\cos\ 2\chi_2)+(\cos 2\chi_3-\cos 2\chi_4)\right] , \tag{30}$$

$$\overline{V} = 0 \quad . \tag{31}$$

In all cases reported here, $|f_2-f_1|<<f_2$ and $|f_4-f_3|<<f_3$, so we can write

$$f_2-f_1 = -\frac{f^3}{2A}(\chi_2-\chi_1) \quad \text{and} \quad f_4-f_3 = -\frac{f^3}{2A}(\chi_4-\chi_3). \tag{32}$$

The polarization fraction of the total radiation can now be calculated from the relation

$$m = \frac{\overline{I}_p}{\overline{I}} = (\overline{Q}^2+\overline{U}^2+\overline{V}^2)^{1/2}/\overline{I} \quad , \tag{33}$$

and is found to be

$$m = m_o \frac{\sin\theta}{\theta} \cos\left[\frac{(\chi_1+\chi_2)-(\chi_3+\chi_4)}{2}\right] \quad , \tag{34}$$

where $\theta=\chi_2-\chi_1=\chi_4-\chi_3$. The quantity m_o is the polarization fraction which would be measured by a receiver of zero bandwidth.

If a source has been observed at three or more frequencies, we can, using equation (34), correct for the effect of the bandwidth. With a single exception this correction was found to be negligible. The sole exception was 3C-161, whose polarization fraction at 1420 Mc/s was corrected from the measured value of 5.8 per cent to the tabulated value of 5.9 per cent.

The negligible influence of the finite bandwidth was also demonstrated experimentally. The 1420-Mc/s receiver was modified to reject one sideband, and the width of the remaining sideband was reduced to approximately

700 kc/s. The sources 3C-123, 3C-196, 3C-295, Hercules A, and 3C-353 were studied. No significant change from our previous results was detected.

CHAPTER III

Discussion of the Measurements

Polarization measurements of radio sources have now been made at several frequencies by various investigators (references 10 through 16 and 24 through 28). The known results for each source can be combined to yield additional useful information.

Faraday Rotation

It is well known that the plane of polarization of an electromagnetic wave is rotated when passing through a medium containing both an ionized gas and a magnetic field with a component along the direction of propagation of the wave. This rotation, called Faraday rotation, is caused by the difference in optical path length between the ordinary and extraordinary waves. In a region containing N_e electrons per cm^3 and a magnetic field B in gauss inclined at an angle α to the direction of propagation, the quasi-longitudinal approximation to the magneto-ionic theory specifies that the amount of rotation θ in radians at a wavelength of λ meters is given by (22),(29)

$$\theta = 8.1 \times 10^5 \lambda^2 \int N_e B \cos\alpha \, dZ \ , \qquad (35)$$

where Z is measured in parsecs along the direction of propagation. Following Gardner and Whiteoak (13), we call the quantity θ/λ^2 the rotation measure. A positive rotation

measure indicates that the magnetic field is directed towards the observer.

The value of the rotation measure is obtained experimentally by measuring the position angle of the plane of polarization at a minimum of three frequencies. Figures 3 through 6 contain a number of graphs in which the abscissa is the square of the wavelength and the ordinate is the polarization position angle. Points on these graphs were supplied by a number of observers. Different symbols have been adopted to distinguish the various contributors.

For all sources the data points are fitted very well by a straight line, the slope of which, when expressed in units of radians/meter^2, is the rotation measure. Extrapolation of the line to $\lambda=0$ gives the intrinsic polarization angle at the source, that is the angle which would be measured in the absence of any intervening magneto-ionic medium.

The rotation measures and intrinsic polarization angles for twenty-five sources are included in Table 2. The values for Fornax A, Pictor A, 3C-270, 3C-279, Centaurus A, 13S6A, 21-64, and 23-64 are those determined by Gardner and Whiteoak (13). For the source 3C-111, independent determinations by two different individuals resulted in different values for the rotation measure and the intrinsic polarization angle. It is possible that the tabulated values of these quantities should be -15 radians/meter^2 and 142°.

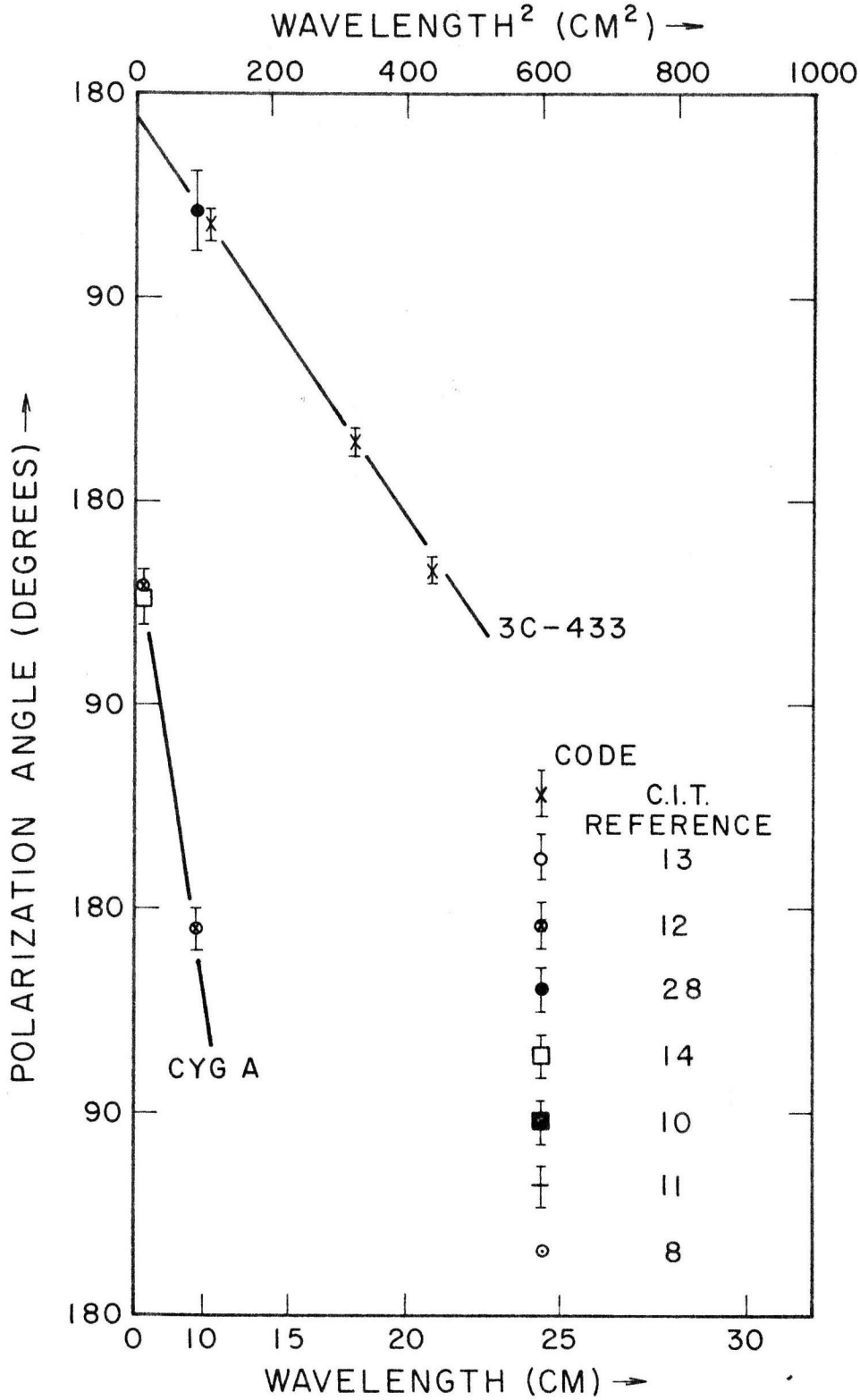

Figure 3. Rotation of the plane of polarization with wavelength.

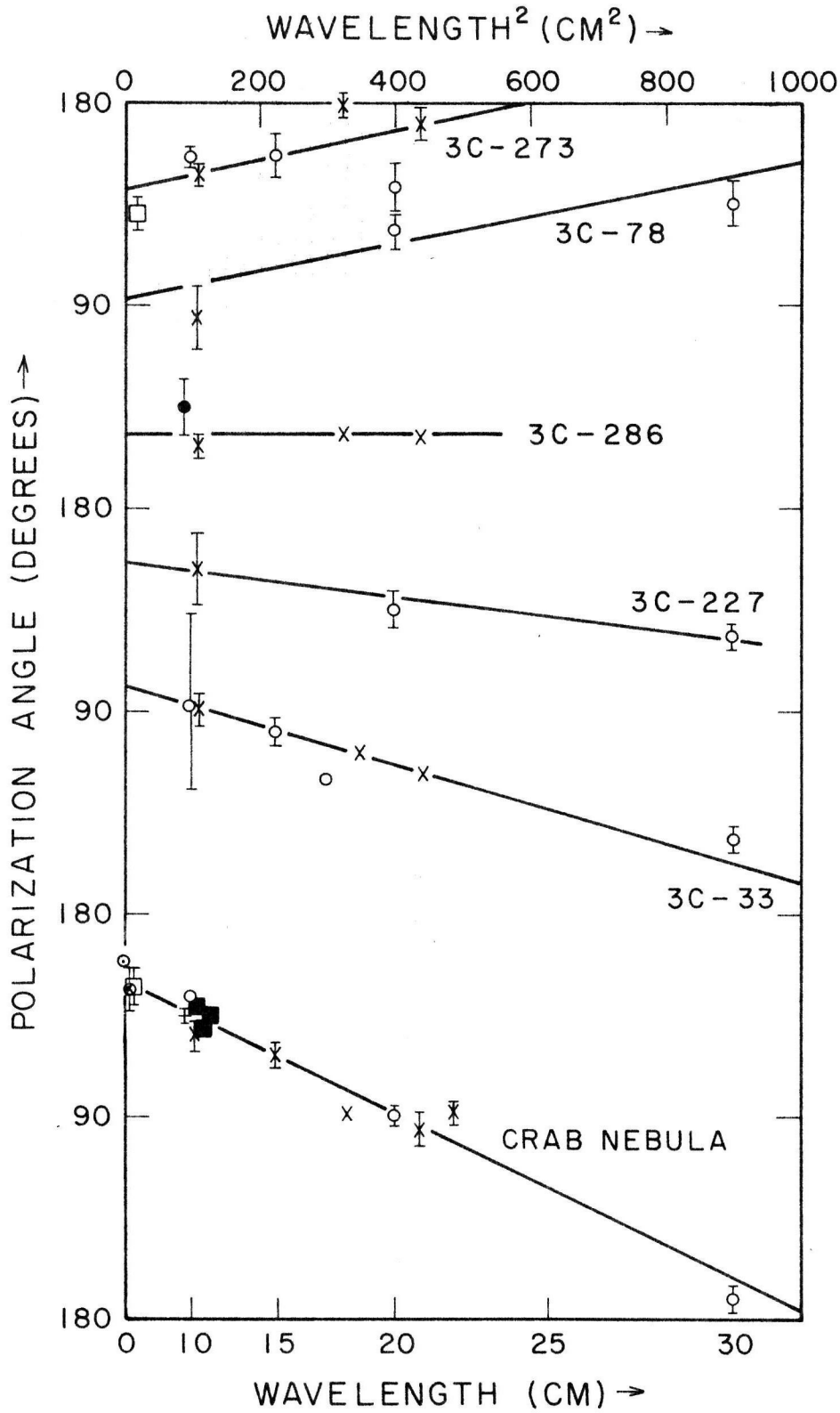

Figure 4. Rotation of the Plane of polarization with wavelength.

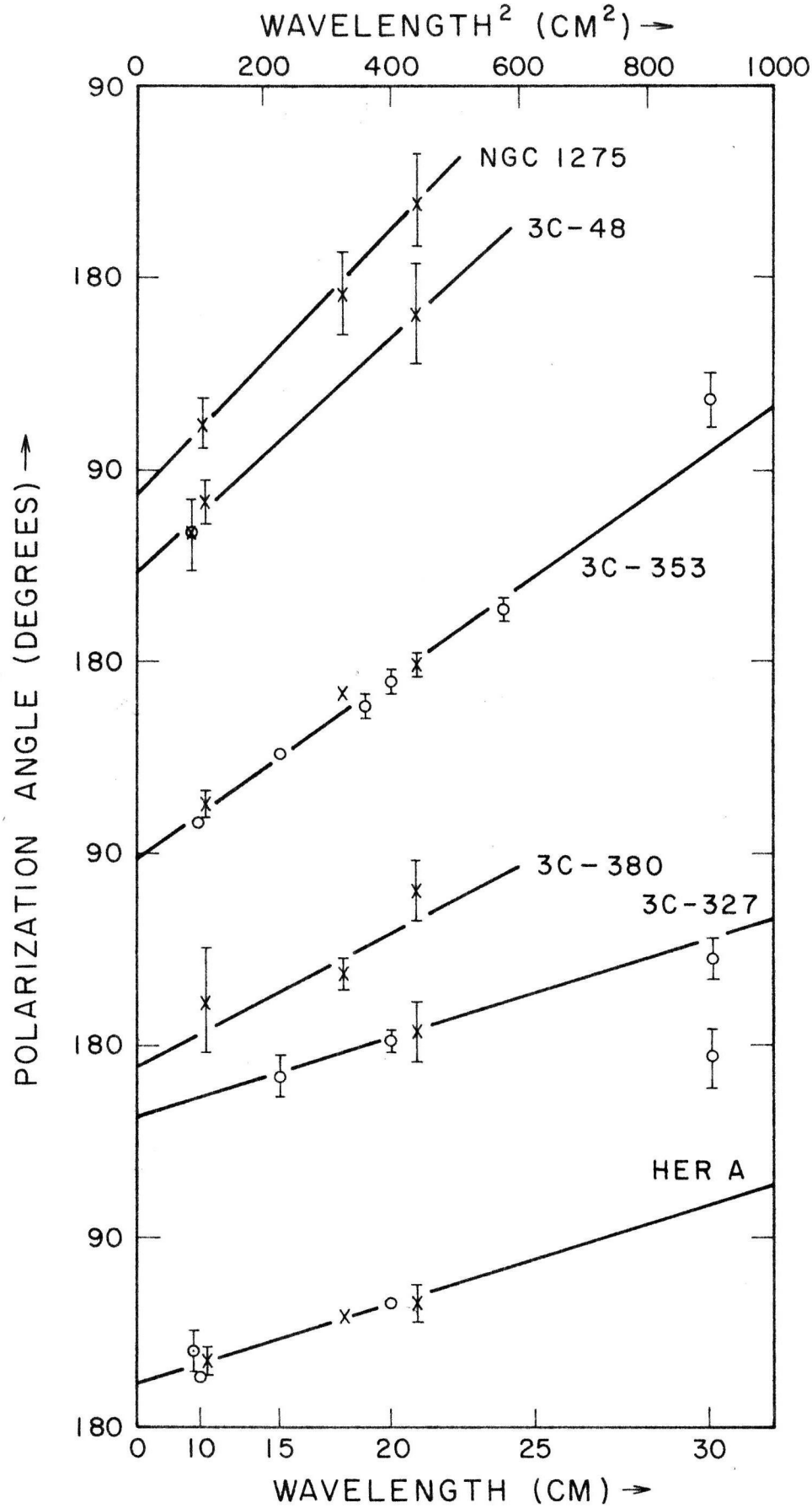

Figure 5. Rotation of the plane of polarization with wavelength.

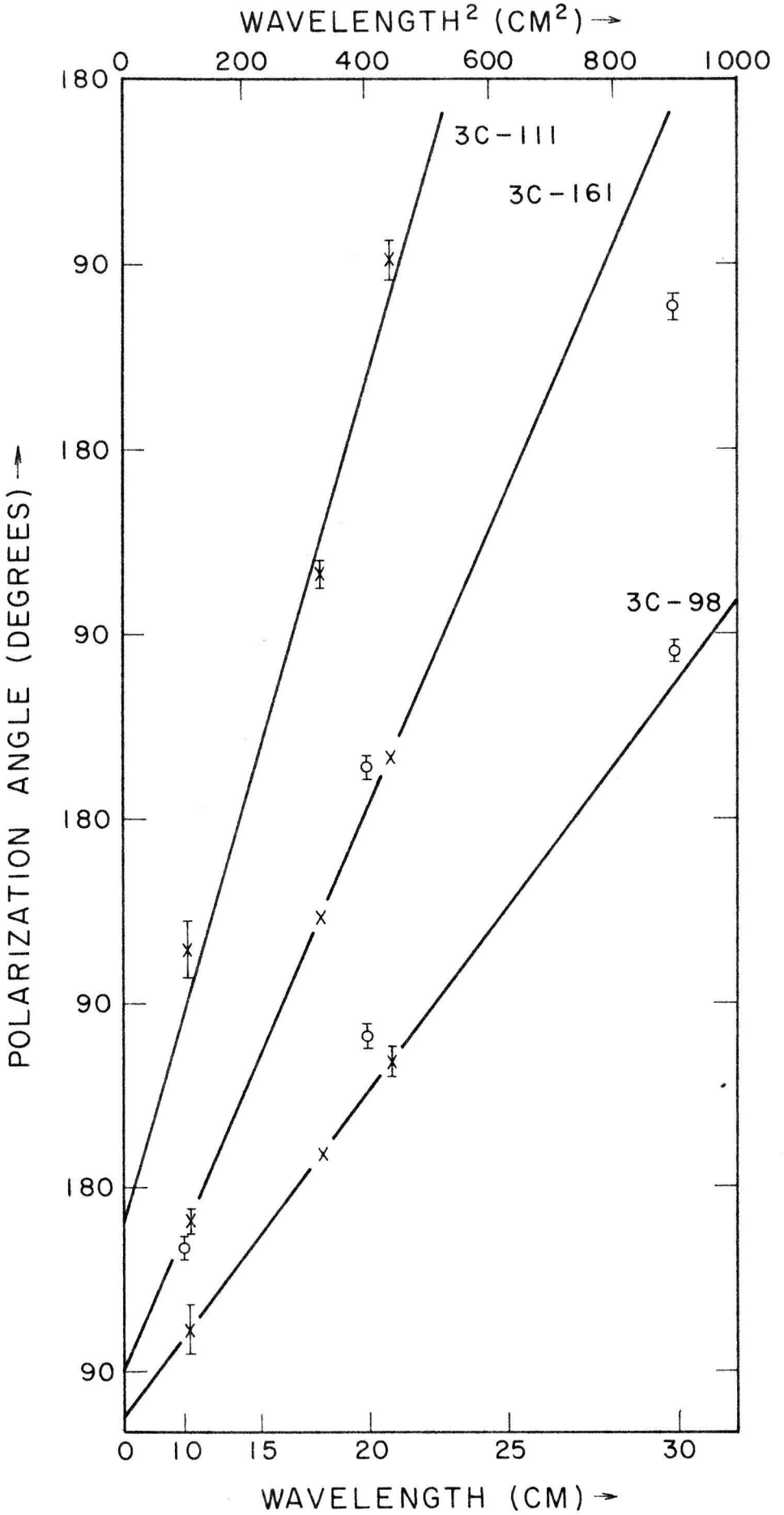

Figure 6. Rotation of the plane of polarization with wavelength.

Table 2. Properties of Linearly Polarized Radio Sources

Source	Galactic Coordinates		Distance	Brightness Temp. at 20 cm	Magnetic Field, H	Intrinsic Pol. Angle	Rotation Measure	Depol. Rate at 20 cm
	l^{II}	b^{II}						
	deg	deg	mpc	^{o}K	oersted	deg	radians m^{-2}	$10^{-3}cm^{-1}$
3C-33	129	-49	178	$4.4x10^{3}$	$3x10^{-4}$	101± 6	-10± 2	0.96±0.50
3C-48	134	-29	1100	$5.0x10^{7}$		40± 7	48± 9	-3.04±1.33
3C-78	175	-45	98	$4.3x10^{4}$	$3x10^{-5}$	92±20	11± 3	0.43±1.70
NGC 1275	151	-13	54	$4.2x10^{3}$	$1x10^{-4}$	76±10	55± 8	-1.36±1.62
For A(a)[1]	240	-57	17		$8x10^{-6}$	66	-2	-3.39±0.53
For A(b)[1]					$8x10^{-6}$	103	-1	-1.01±1.16
3C-98	180	-31	92	$1.0x10^{3}$	$3x10^{-5}$	66±10	70± 3	-1.87±0.58
3C-111	162	-9		$1.9x10^{3}$		160±20	180±10	-0.93±1.56
Pic A	251	-34	100	$9.0x10^{2}$		110	45	-0.50±0.54
Crab Neb.	185	-6	$1.03 x10^{-3}$	$1.6x10^{4}$		150± 5	-25± 4	-0.91±0.06
3C-161	215	-8		$1.6x10^{5}$		88±10	121±15	
3C-227	229	42		$1.5x10^{3}$		159±12	-6± 3	2.67±0.27
3C-270	282	67	11	$6.2x10^{2}$	$3x10^{-5}$	105	4± 2	-1.04±0.70
3C-273	290	64	474		$1.5x10^{-4}$	141±10	11± 6	-1.39±0.67
3C-279[2]	307	57				126	10± 3	4.08±1.42

Table 2 (continued)

Source	Galactic Coordinates		Distance	Brightness Temp. at 20 cm	Magnetic Field, H	Intrinsic Pol. Angle	Rotation Measure	Depol. Rate at 20 cm
	ℓ^{II}	b^{II}						
	deg	deg	mpc	^{o}K	oersted	deg	radians m^{-2}	$10^{-3}cm^{-1}$
Cen A(a)[3]	310	20	4.7	4.5×10^{3}	8×10^{-5}	147	-60	-1.99 ± 1.42
Cen A(b)[3]					6×10^{-6}	56	-68	
Cen A(c)[3]					6×10^{-6}	172	-66	
3C-286	57	81		8.4×10^{6}		33 ± 5	0 ± 3	0.27 ± 1.08
1356 A	310	2				20	59	-3.85 ± 1.00
3C-327	12	38	309	1.4×10^{3}	2×10^{-5}	145 ± 5	16 ± 3	-0.38 ± 1.08
Her A	23	29	462	1.9×10^{4}	5×10^{-5}	21 ± 7	16 ± 4	-0.83 ± 0.18
3C-353	21	20	87	6.1×10^{3}	4×10^{-5}	87 ± 3	37 ± 4	-3.82 ± 0.57
3C-380	77	24		1.4×10^{5}		168 ± 10	28 ± 10	0.39 ± 1.38
Cyg A	76	6	171	3.1×10^{5}	2×10^{-5}	166 ± 10	-338 ± 50	
3C-433	75	-18	304	4.4×10^{4}	3×10^{-5}	171 ± 6	-78 ± 4	0.0 ± 1.33
21-64	321	-41				28	30	-2.35 ± 0.30
23-64	314	-55				11	23	-0.72 ± 0.17

1. Fornax A(a) is the larger component at $\alpha = 03^{h}\ 20^{m}.5$, $\delta = -37^{o}\ 18'$; (b) is the smaller component at $\alpha = 03^{h}\ 22^{m}.7$, $\delta = -37^{o}\ 18'$.
2. Measurements available at only two frequencies.
3. Centaurus A(a) is the central component at $\alpha = 13^{h}\ 23^{m}.2$, $\delta = -42^{o}\ 48'.5$; (b) is at $\alpha = 13^{h}\ 24^{m}.0$, $\delta = -42^{o}\ 30'$; (c) is at $\alpha = 13^{h}\ 20^{m}.5$, $\delta = -44^{o}\ 25'$.

Table 2 also contains some additional physical properties of the sources. The brightness temperatures were provided by Kellermann (30). The magnetic fields for most of the sources were taken from Maltby, Matthews, and Moffet (31). The field calculations for NGC 1275, 3C-273, and 3C-433 were performed in an identical manner to that used by these authors. The depolarization rate will be defined later.

It is worth noting that, of the twenty-five sources studied, only seven have negative rotation measures. One has a rotation measure of zero, and the remaining seventeen are positive. The sources with negative rotation measures are scattered throughout the system of galactic coordinates in no obvious pattern. It is felt that the number of sources for which data are presently available is too limited to permit conclusions regarding the nature of the galactic magnetic field.

There are several magneto-ionic media in which the measured Faraday rotation could take place. The earth's ionosphere can make only a very small contribution. Hatanaka (22) has estimated the rotation which occurs in the ionosphere to be approximately 6 radians at 200 Mc/s, corresponding to a rotation measure of 2.7 radians/meter^2. This estimate was based on the assumption that the magnetic field is everywhere parallel to the line of sight; hence it represents a probable upper limit. Cooper and Price (26) have detected no change in the polarization angle of Centaurus A during observations extending from afternoon

until midnight, although the electron content of the ionosphere changes considerably during this interval.

Sciama (32) has proposed that the Faraday rotation observed for Centaurus A takes place in the local cluster of galaxies. Because of existing uncertainties in the values of ionized-gas density, magnetic field, and dimensions in the local cluster, however, it appears possible to calculate rotation measures of any magnitude. We therefore do not consider this a fruitful suggestion, nor a necessary one in light of the arguments to be developed later.

It has also been suggested (32) that intergalactic space may contain a sufficient particle density and magnetic field to account for the observed rotation measures. One would then expect the rotation measure to depend strongly on distance, an increase in one implying an increase in the other. No such dependence is evident in Figure 7, where |rotation measure| is plotted against distance. We therefore reject intergalactic space as the primary source of rotation.

Cooper and Price (26), from their observations of Centaurus A, believed the majority of the rotation to occur either in our Galaxy or in the outer regions of the emitting source. They point out that the rotation measures determined at three points in the source spanning a distance of 160 kiloparsecs differ only slightly. Fornax A has also been observed at two points separated by approximately 160 kiloparsecs (13), and again the rotation measures are very nearly identical. Since it is difficult to conceive of a

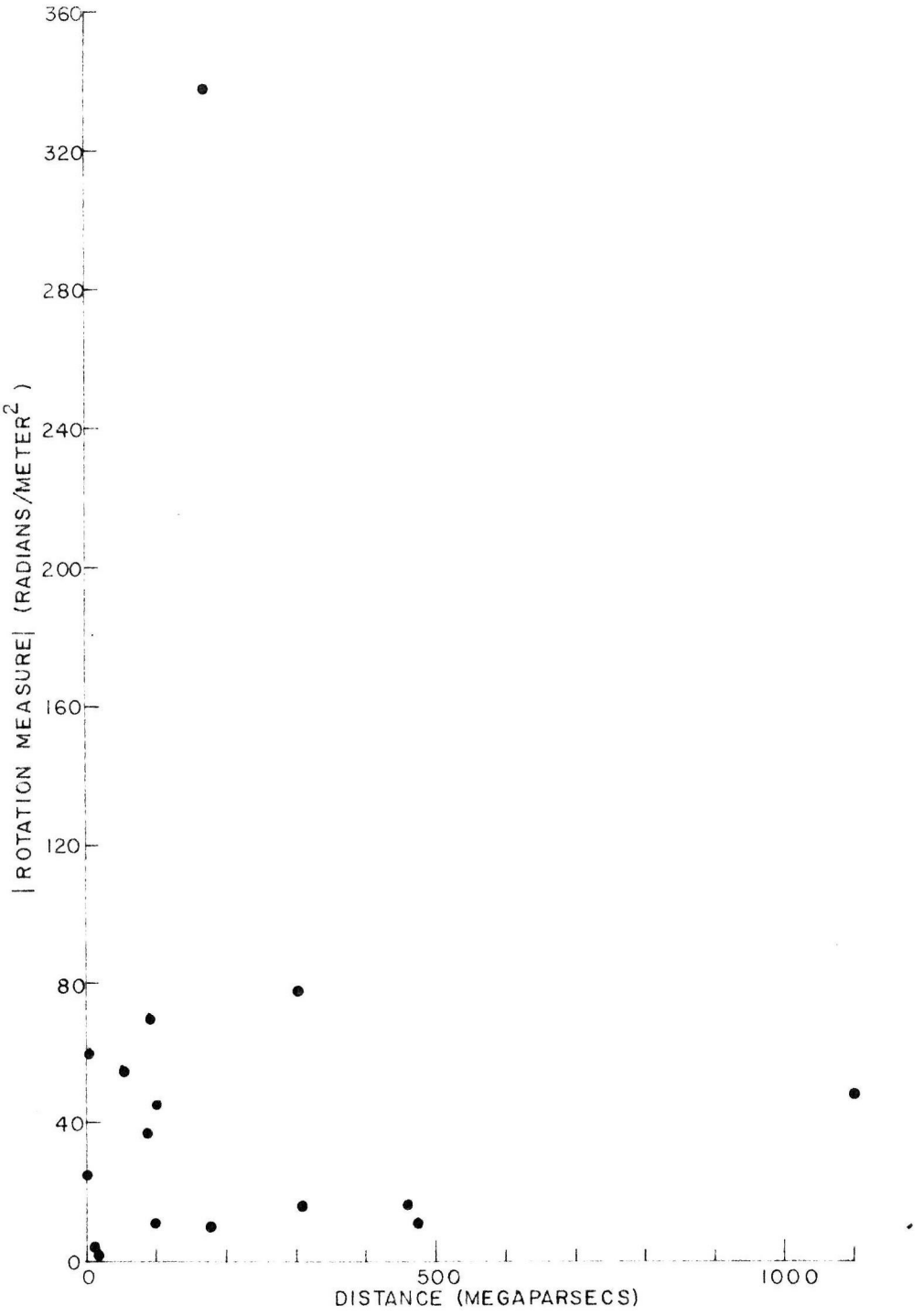

Figure 7. Plot of |rotation measure| vs. distance to the emitting source.

uniform medium extending over such vast dimensions, it appears unlikely that the observed rotation is occurring in the outer regions of the emitting sources.

Gardner and Whiteoak (13), using observations of eighteen sources, point out that the sources with small rotation measures are at high galactic latitudes. For the sources at low and intermediate latitudes, they find a scatter in both magnitude and sign of the rotation measures. Their results, combined with those reported here, strongly suggest that the majority of the observed Faraday rotation occurs within our own Galaxy.

Figure 8 illustrates the variation of the observed rotation measures with galactic coordinates. The size of the circles indicates the value of the rotation measure, increasing size denoting large rotation measures. Open circles represent negative rotation measures and filled circles the opposite. The numbers in parentheses are the rotation measures in radians/meter^2.

It is seen that all seven of the sources in the category of smallest absolute rotation measure lie at latitudes greater than 42°. Also, all three of the sources in the category of largest absolute rotation are within 8° of the galatic equator. The sources in the middle two categories are scattered between $b^{II} = +38°$ and $b^{II} = -41°$.

The dependence on galactic latitude is also well illustrated in Figure 9, where cosecant $|b^{II}|$ is the abscissa

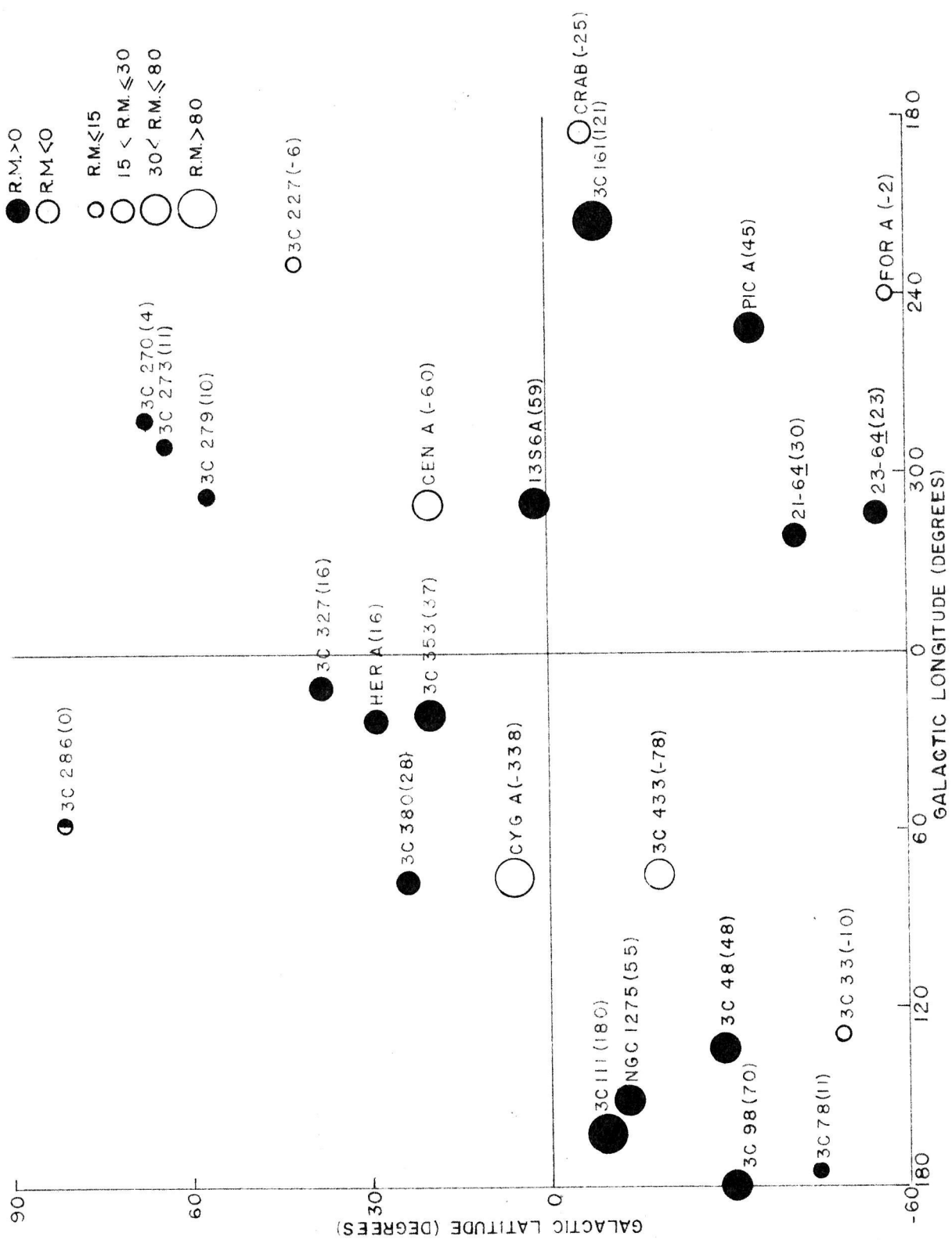

Figure 8. Rotation measures on a system of galactic coordinates. The numbers in parentheses are the rotation measures in radians/meter^2.

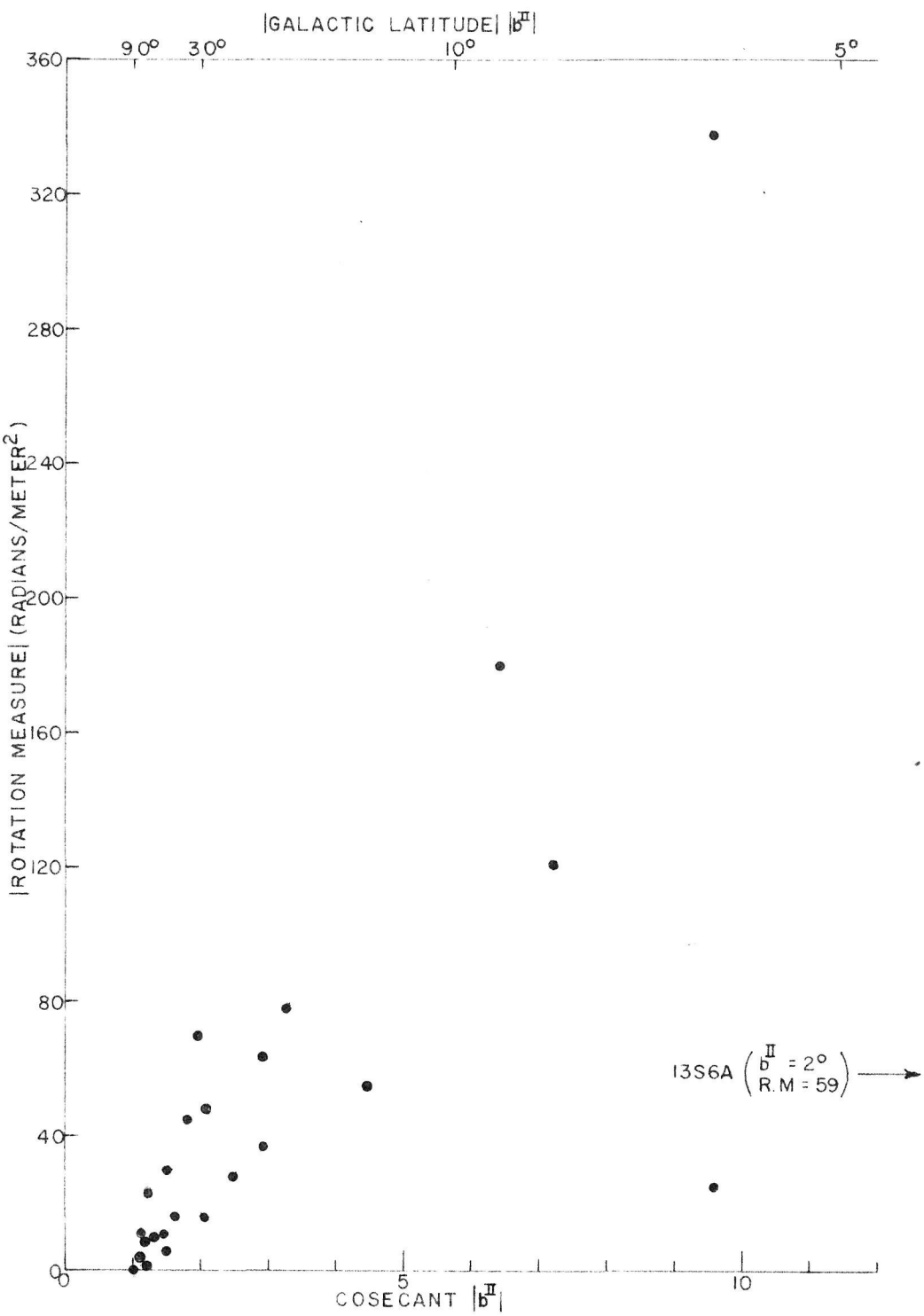

Figure 9. Dependence of | rotation measure | on cosecant of | galactic latitude |.

and |rotation measure| is the ordinate. In general, increasing cosecant $|b^{II}|$, corresponding to decreasing $|b^{II}|$, implies increasing absolute rotation measure. The only exceptions to this relation are the Crab Nebula and 13S6A. One of these is known to be a galactic source, and the other is very likely such. Since the path length through the Galaxy of a signal emitted by these sources is therefore less than for the extragalactic sources, it is not surprising that their rotation measures are relatively smaller.

The above evidence strongly suggests that most of the observed Faraday rotation occurs in our own Galaxy. It should therefore be possible to derive properties of the Galaxy from the observed rotation measures. For instance, if the dimensions of the Galaxy are known, one can compute average values of the product of the charged-particle density N_e and the line-of-sight magnetic field $B_{||}$.

To perform this calculation we have constructed a model of the Galaxy consisting of a uniform disk and a spherical halo (see Figure 10). The halo and the disk each have a radius of 12 kiloparsecs, and the thickness of the disk is 300 parsecs. The sun lies in the median plane of the disk at a distance of 10 kiloparsecs from the center. The electron density and the magnetic field in the halo are assumed to be 10^{-2} and 1/3, respectively, of the corresponding values in the disk. Consequently, in calculating the distance traveled through the Galaxy by the signal emitted by a source

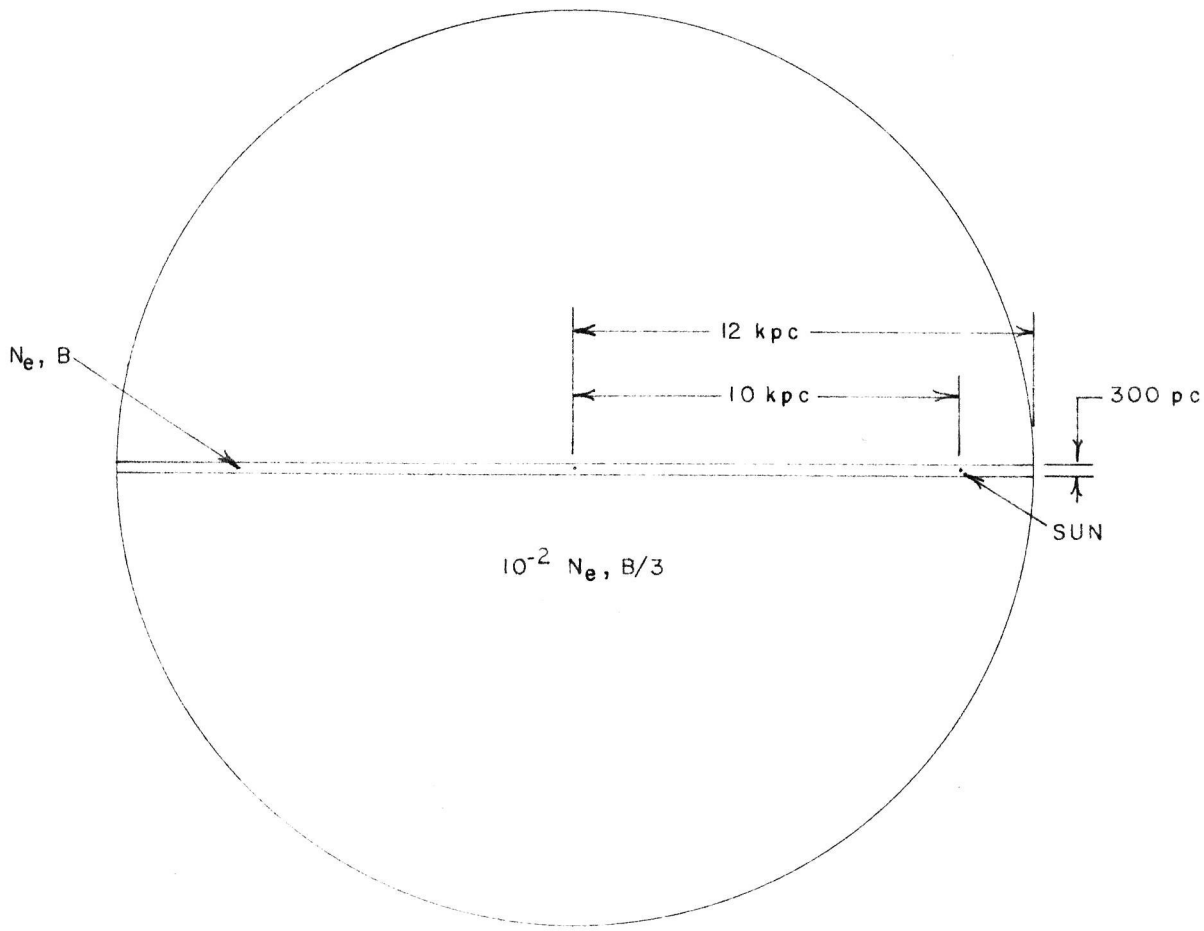

Figure 10. Assumed model of the Galaxy.

of known galactic coordinates, relative weights of 300 and 1 have been assigned to the path lengths through the disk and the halo respectively.

The calculations are summarized in Table 3. Next to each source are the path lengths through the disk and through the halo. The distance to the Crab Nebula was taken to be 1030 parsecs (33). The source 13S6A was not included, since it is probably galactic, but of unknown distance. We have also computed the sum $(L_{disk}+L_{halo}/300)$. When the rotation measure is divided by the product of this sum with 8.1×10^{5}, the quotient is the average value of the product of the electron density N_e and the line-of-sight magnetic field $B_{||}$ (see equation (35)). This latter quantity is tabulated in column 5 of Table 3.

The products $\overline{N_e B_{||}}$ exhibit a striking latitude dependence. This is evident in Figure 11 where the magnitude and sign of this product are plotted for each source on a galactic coordinate system. The magnitude of $\overline{N_e B_{||}}$ is represented by the size of the circle; the sign is positive for filled circles and negative for open circles. In parentheses beside each source are the numerical values of $\overline{N_e B_{||}}$ in units of 10^{-8} gauss cm^{-3}.

We have illustrated the dependence of $\overline{N_e B_{||}}$ on galactic latitude in two additional ways. Figure 12 plots the absolute value of $\overline{N_e B_{||}}$ as a function of absolute galactic latitude. Excluding the Crab Nebula, there is a definite tendency for $|\overline{N_e B_{||}}|$ to decrease as $|b^{II}|$ increases.

Table 3. Features of the Galaxy

Source	L_{disk}(pc)	L_{halo}(pc)	$L_{disk}+L_{halo}/300$ (pc)	$N_e B_{ll}$(G cm^{-3})
3C-33	200	3450	210	-5.9×10^{-8}
3C-48	310	2690	320	18.5
3C-78	210	2490	220	6.2
NGC 1275	670	1570	670	10.1
Fornax A	180	4450	200	-0.9
3C-98	290	1910	300	7.0
3C-111	960	1390	960	23.2
Pictor A	270	4330	280	19.8
Crab Nebula	1030	0	1030	-3.0
3C-161	1080	1260	1080	13.8
3C-227	220	2080	230	-4.8
3C-270	160	7280	180	2.7
3C-273	170	8080	200	6.8
3C-279	180	10520	220	5.6
Centaurus A	440	14621	490	-15.9
3C-286	150	745	170	0.0
3C-327	240	17710	300	6.6
Hercules A	310	18070	370	5.3
3C-353	440	19370	500	9.1
3C-380	370	8760	400	8.6
Cygnus A	1430	8170	1460	-28.6
3C-433	490	8600	520	-18.5
21-64	230	14520	280	13.2
23-64	180	11470	220	12.9

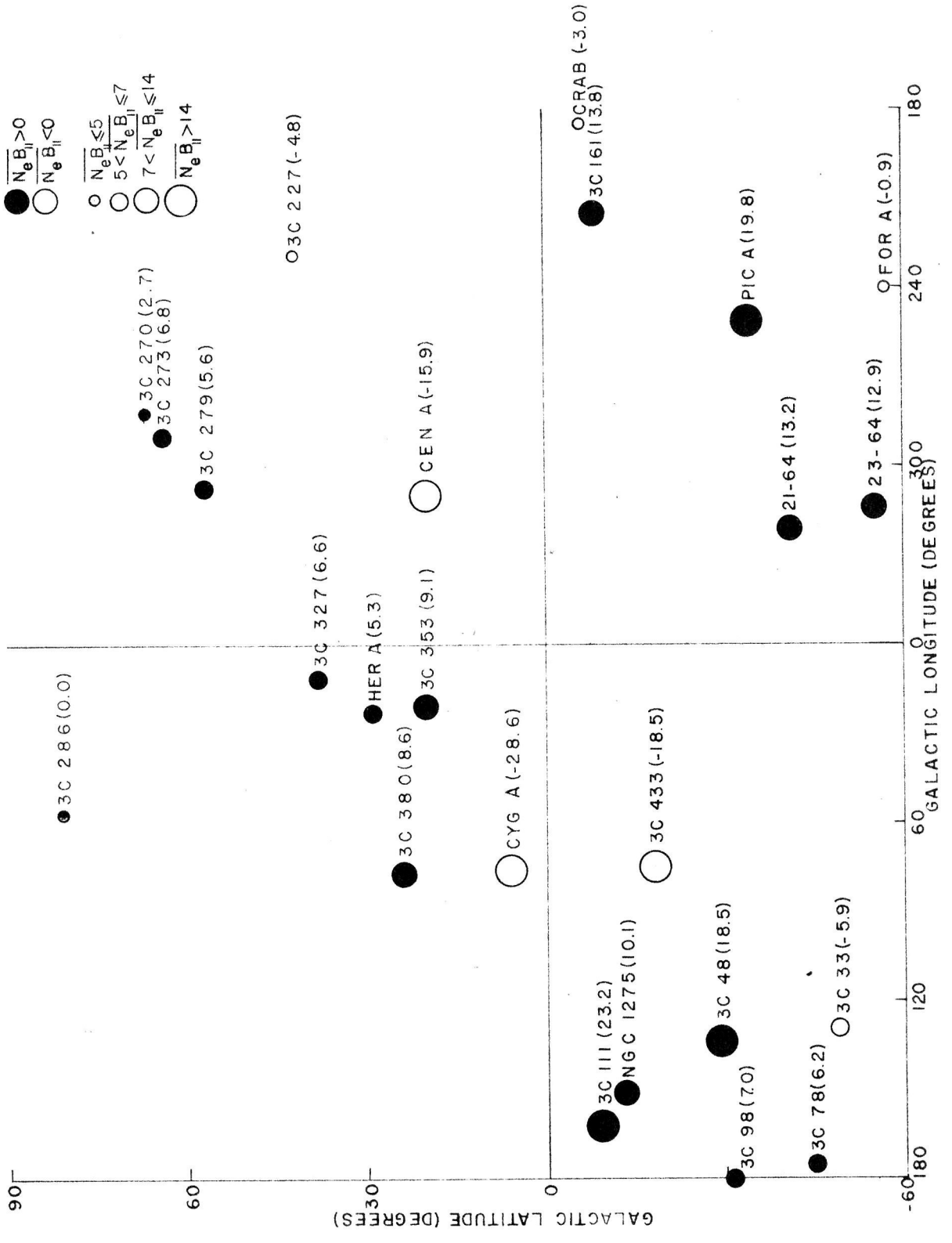

Figure 11. Average products of electron density and longitudinal magnetic field on a system of galactic coordinates. The numbers in parenthesis are the values of $N_e B_{||}$ in units of 10^{-8} Gauss cm^{-3}.

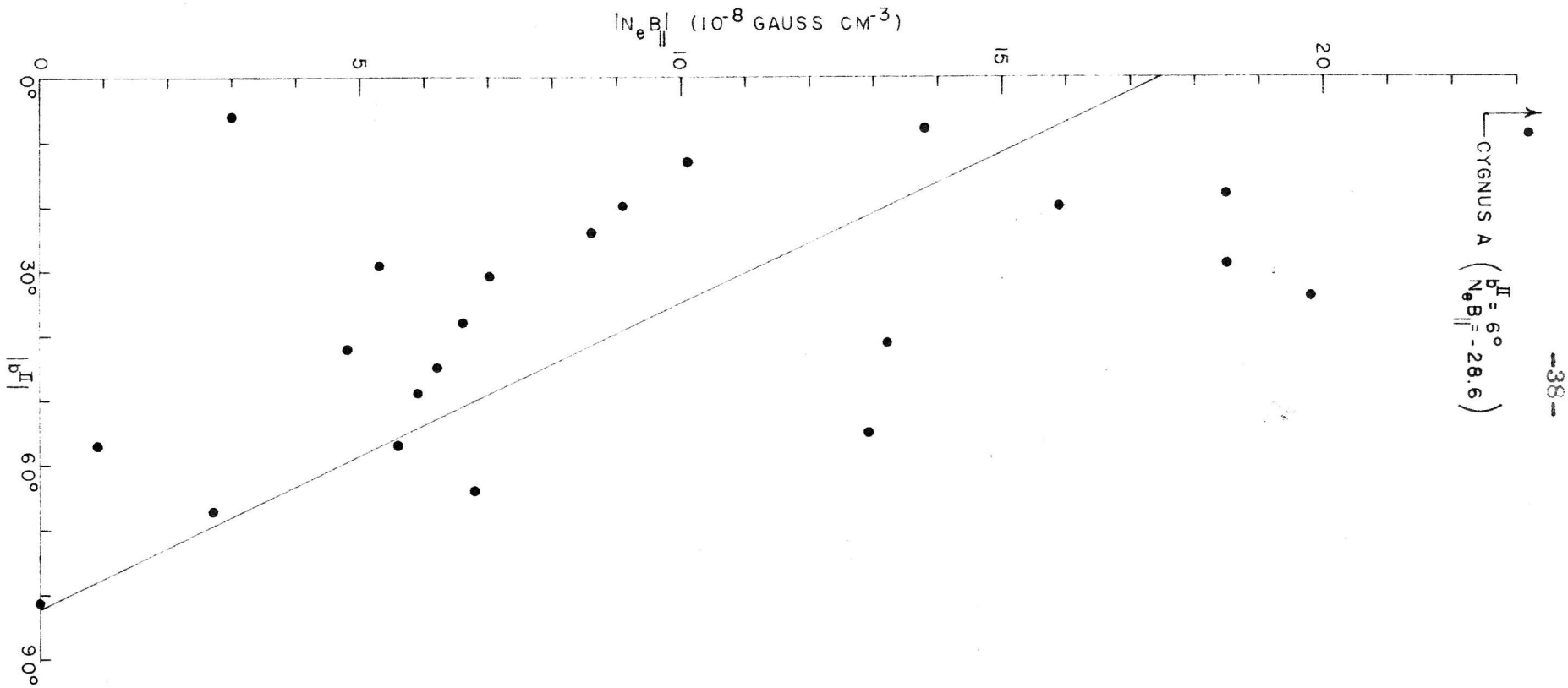

Figure 12. Dependence of average product of electron density and longitudinal magnetic field on galactic latitude. The solid line passes through points representing the average of all sources within a 20°-interval of galactic latitude.

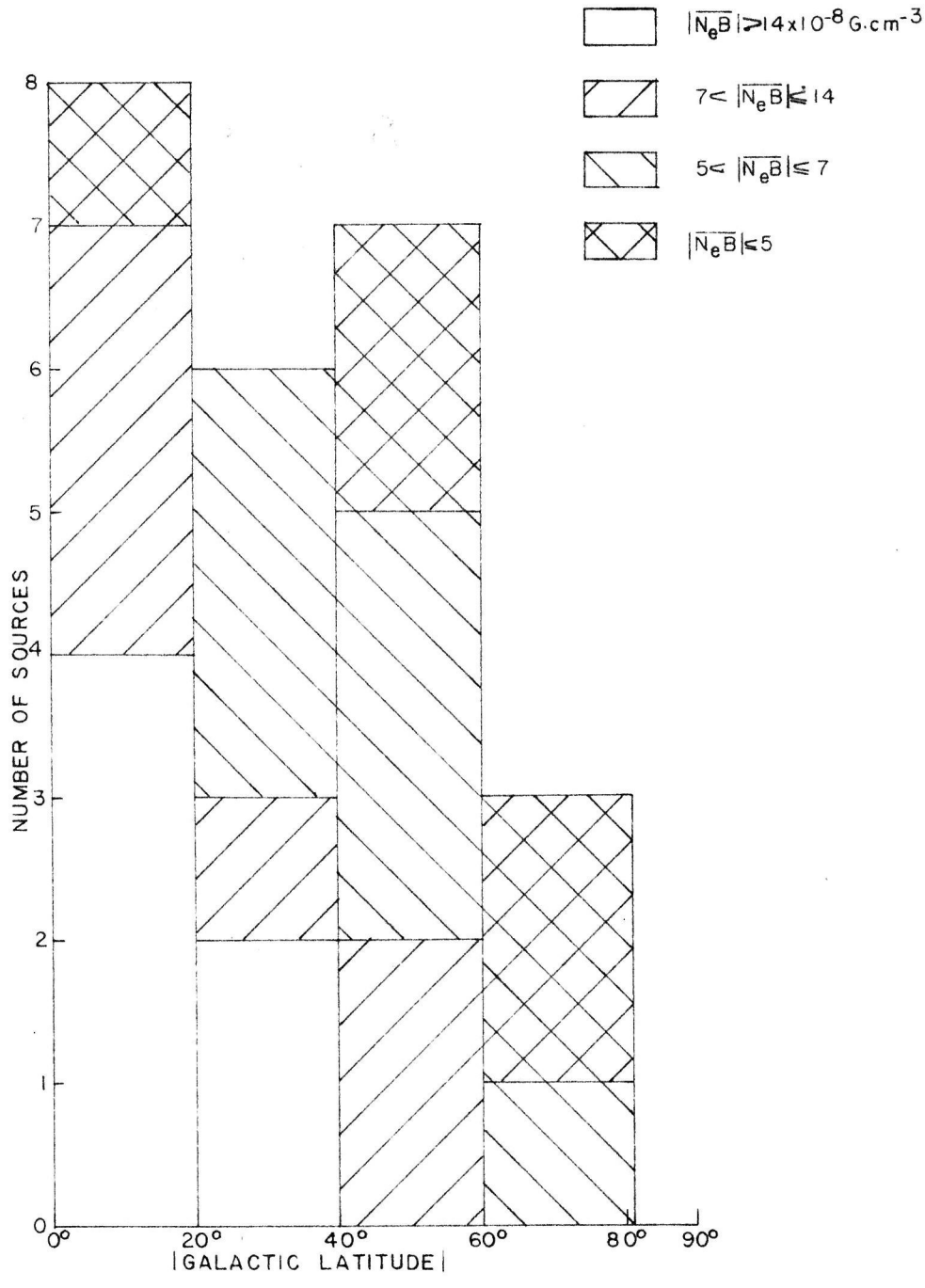

Figure 13. Histogram showing distribution of classes of average products of electron density and longitudinal magnetic field.

Figure 13 is a histogram in which the distribution of the four groups of values of $|\overline{N_e B_{||}}|$ is illustrated. Again the Crab presents the only notable irregularity.

Finally, we have computed average values of the magnitudes of $\overline{N_e B_{||}}$ in four zones of galactic latitude. The results are presented in Table 4. A steady decrease in magnitude with increase in latitude is noted. The relation is very nearly linear, and has been plotted in Figure 12.

Table 4. Latitude Dependence of $|\overline{N_e B_{||}}|$

Galactic Zone	Number of Sources, n	$(\Sigma \lvert N_e B_{\|\|} \rvert)/n$
$0 \leq \lvert b^{II} \rvert \leq 20$	8	15.3×10^{-8} Gauss cm^{-3}
$20 \leq \lvert b^{II} \rvert \leq 40$	6	11.0
$40 \leq \lvert b^{II} \rvert \leq 60$	7	7.1
$60 \leq \lvert b^{II} \rvert \leq 81$	3	3.2

Depolarization Rate

It is readily apparent that the percentage polarization changes with wavelength more rapidly for some sources than for others. Figures 14 and 15 show a number of curves in which percentage polarization is plotted against wavelength. The symbols have the same meaning as in Figures 3 through 6. In all cases except 3C-161 a straight line, or sometimes two straight lines, adequately represents the data points. The slope of this line will be called the depolarization rate, and is a measure of how rapidly the degree of

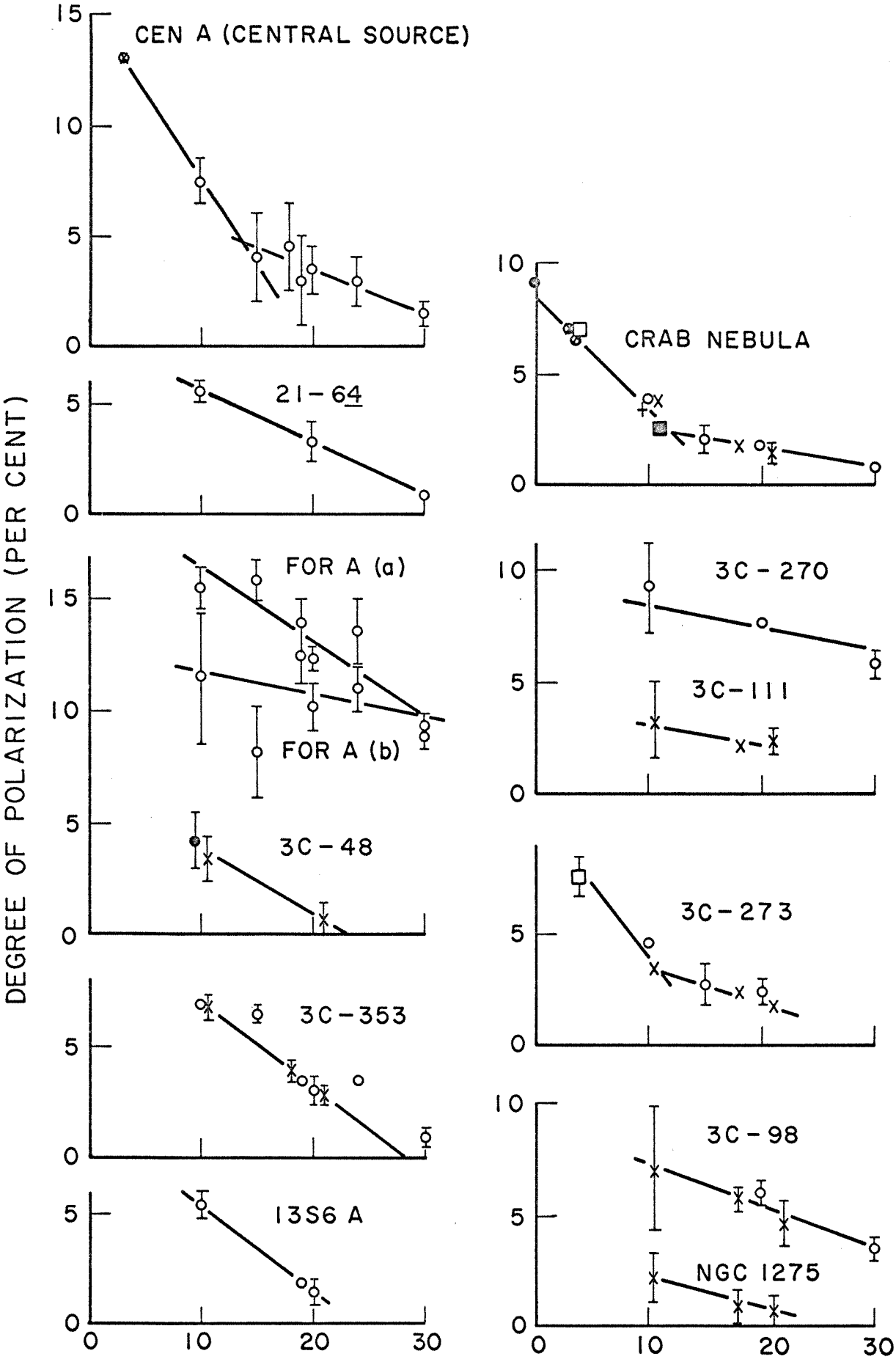

Figure 14. Change of degree of polarization with wavelength. See Fig. 3 for meaning of symbols.

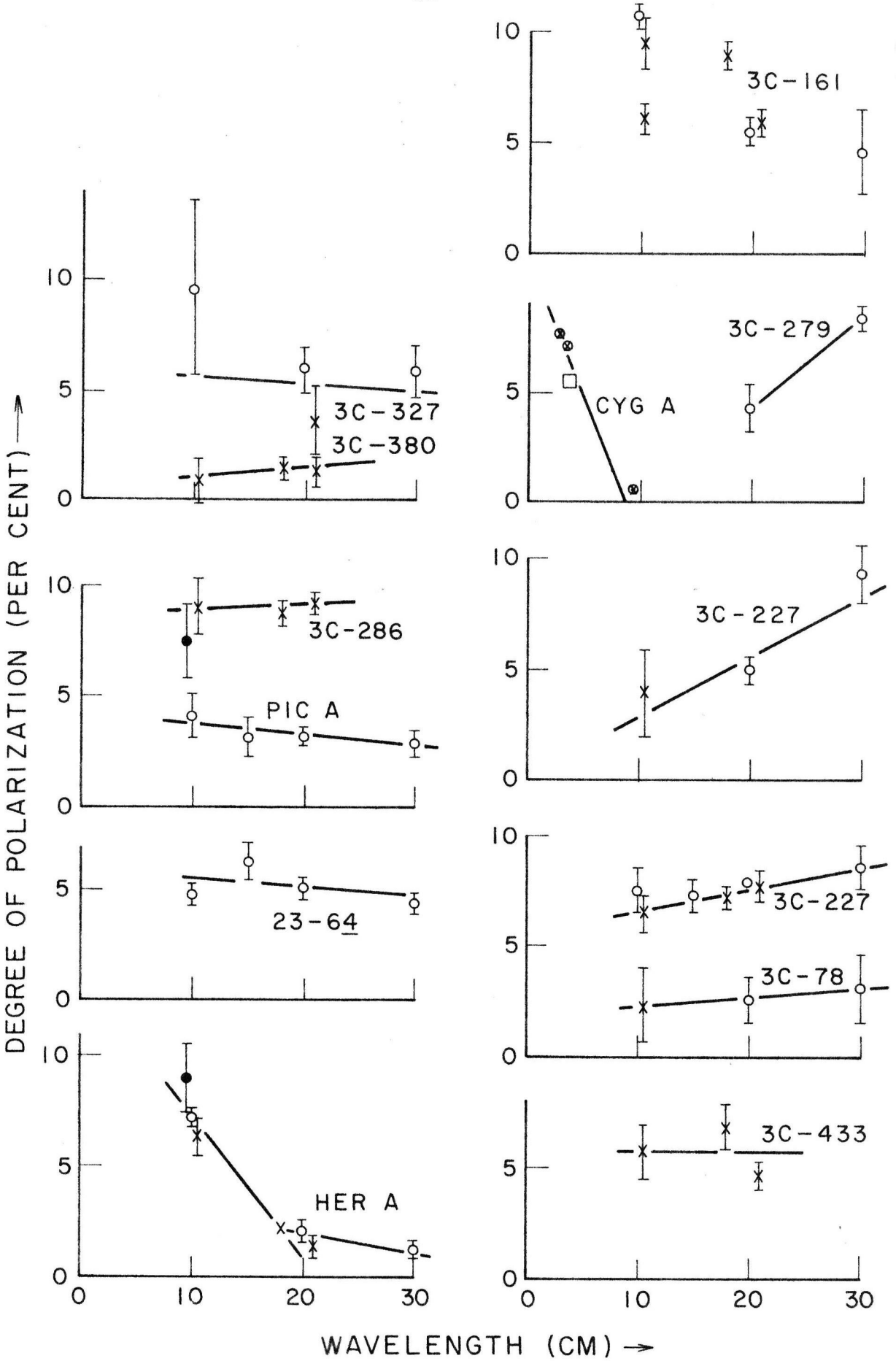

Figure 15. Change of degree of polarization with wavelength. See Fig. 3 for meaning of symbols.

polarization varies with wavelength. When the depolarization rate is negative, the percentage polarization decreases as the wavelength increases; the opposite is true for a positive depolarization rate.

Examination of the sources 3C-273, Hercules A, Cygnus A, the Crab Nebula, and the central component of Centaurus A reveals that at sufficiently high frequencies the polarization increases rapidly. Thus, as shorter wavelengths are approached, there is probably a point at which the depolarization becomes a large negative number for all sources. Since high-frequency (>3000 Mc/s) measurements are available for only a few sources, however, it is not possible to statistically correlate the initial steep decline in polarization with other physical properties of the sources. Consequently the depolarization rate at a wavelength of 20 cm has been chosen for examination. All the following conclusions are valid only for this choice. They may not apply to the depolarization rates at high frequencies.

Gardner and Whiteoak (13) have mentioned the possibility that some depolarization occurs within our Galaxy. It now appears that only a small part, if any, of the observed depolarization at frequencies below 3000 Mc/s can be accounted for by this means.

In Figure 16 the depolarization rates at 20 cm for twenty-three sources are plotted on a system of galactic coordinates. The larger the circle, the greater is the

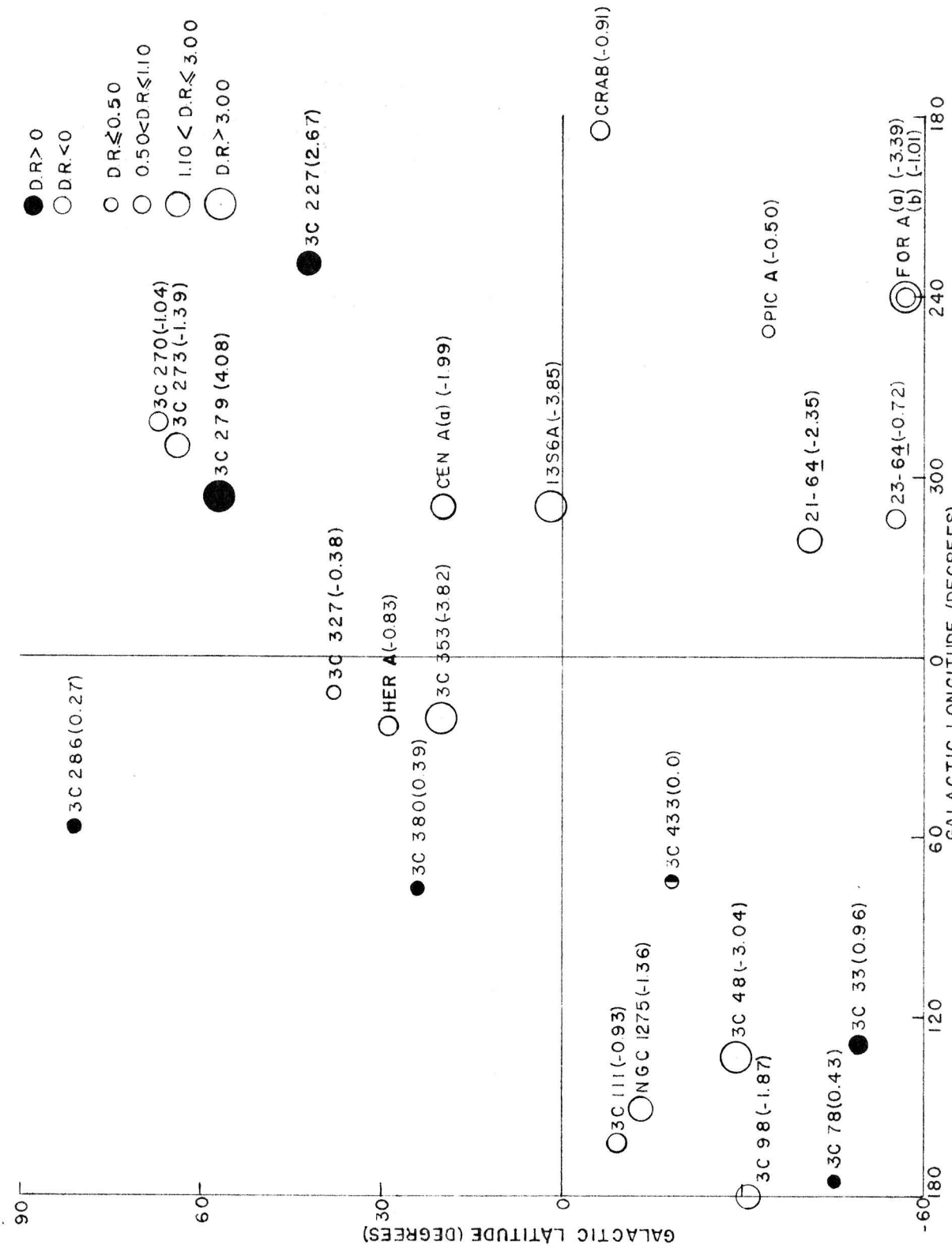

Figure 16. Depolarization rates on a system of galactic coordinates. The numbers in parentheses are the depolarization rates at 20 cm in units of 10^{-3} cm^{-1}.

magnitude of the depolarization rate. Open circles indicate negative depolarization rates and filled circles positive rates. The numbers in parentheses are the rates at 20 cm in units of 10^{-3} cm^{-1} .

The existence of sources with positive depolarization rates is somewhat surprising. For these sources the degree of polarization increases with increasing wavelength. The errors on the depolarization rates of the sources 3C-78, 3C-286, and 3C-380 are large enough that their rates may be zero or even negative. The same cannot be said for the sources 3C-33, 3C-227, and 3C-279, however. The first two of these are double sources; 3C-279 has not been resolved. The assignment of positive depolarization rates to 3C-227 and 3C-279 depends entirely on the results of Gardner and Whiteoak (13). Confirming measurements by independent observers would be very useful.

No dependence on galactic coordinates is evident in Figure 16. For example, the sources 3C-273, 3C-279, and the larger component of Fornax A have both high galactic latitudes ($|b^{II}|>57°$) and large depolarization rates ($|D.R.|>1.39\times10^{-3}cm^{-1}$). The sources 3C-380, 3C-327, and Pictor A, on the other hand, lie at intermediate latitudes ($|b^{II}|<38°$), but have small depolarization rates ($|D.R.|<0.5\times10^{-3}cm^{-1}$).

The absence of a latitude effect is also demonstrated by a plot of |depolarization rate| vs. cosecant $|b^{II}|$ (Figure 17). No apparent correlation exists between these two quantities.

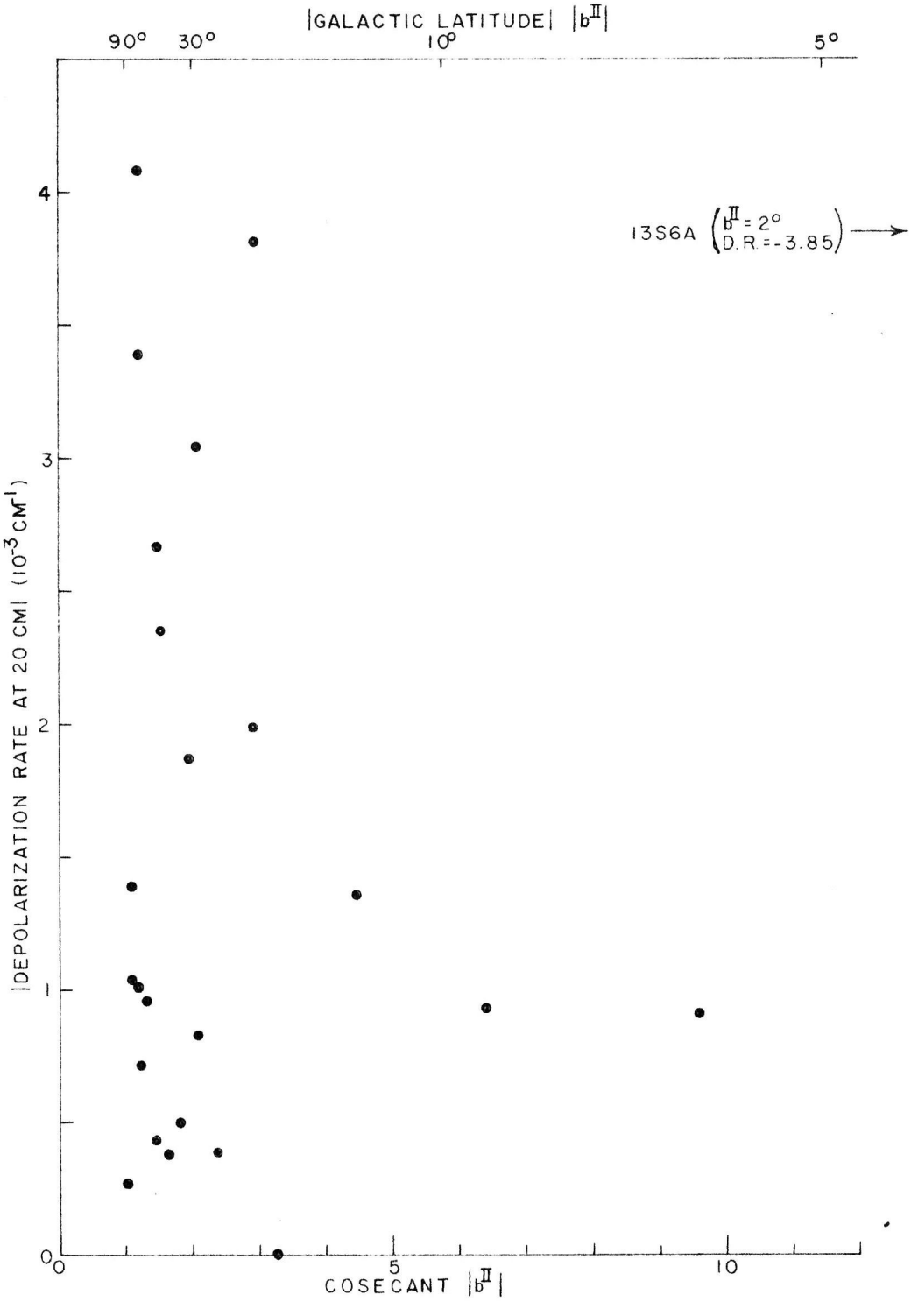

Figure 17. Plot of | depolarization rate at 20 cm | vs. cosecant of | galactic latitude |.

We have previously concluded that the measured rotation measures are properties of our own Galaxy. A large rotation measure implies that the product of particle density and longitudinal magnetic field is likewise large in that region of the Galaxy. If most of the depolarization occurs in the Galaxy, we expect it to be most rapid in regions of large N_e and B. Thus, we expect large rotation measure to imply large depolarization rate. Figure 18, in which rotation measure is the abscissa and depolarization rate the ordinate, fails to exhibit this correlation, again suggesting that the Galaxy is not responsible for the observed depolarization.

It is conceivable that the depolarization of a radio source is a consequence of the different paths traveled through the Galaxy by signals emitted from different regions on the surface of the source. Davies and Verschuur (16) have suggested that this mechanism accounts for the depolarization of Cygnus A between 3 and 21 cm. The angular dimensions of the sources studied, however, are of the order of a few minutes of arc. Moreover, from Table 3 we see that 500 parsecs can be taken as a typical distance along which the Galaxy can produce a significant effect. An angle of 5' corresponds to a physical dimension of 0.7 parsecs at a distance of 500 parsecs. Thus, unless irregularities in the structure of the galactic magnetic field and/or ionized-gas distribution exist over lengths of the order of a parsec, the observed depolarization cannot be accounted for by this means.

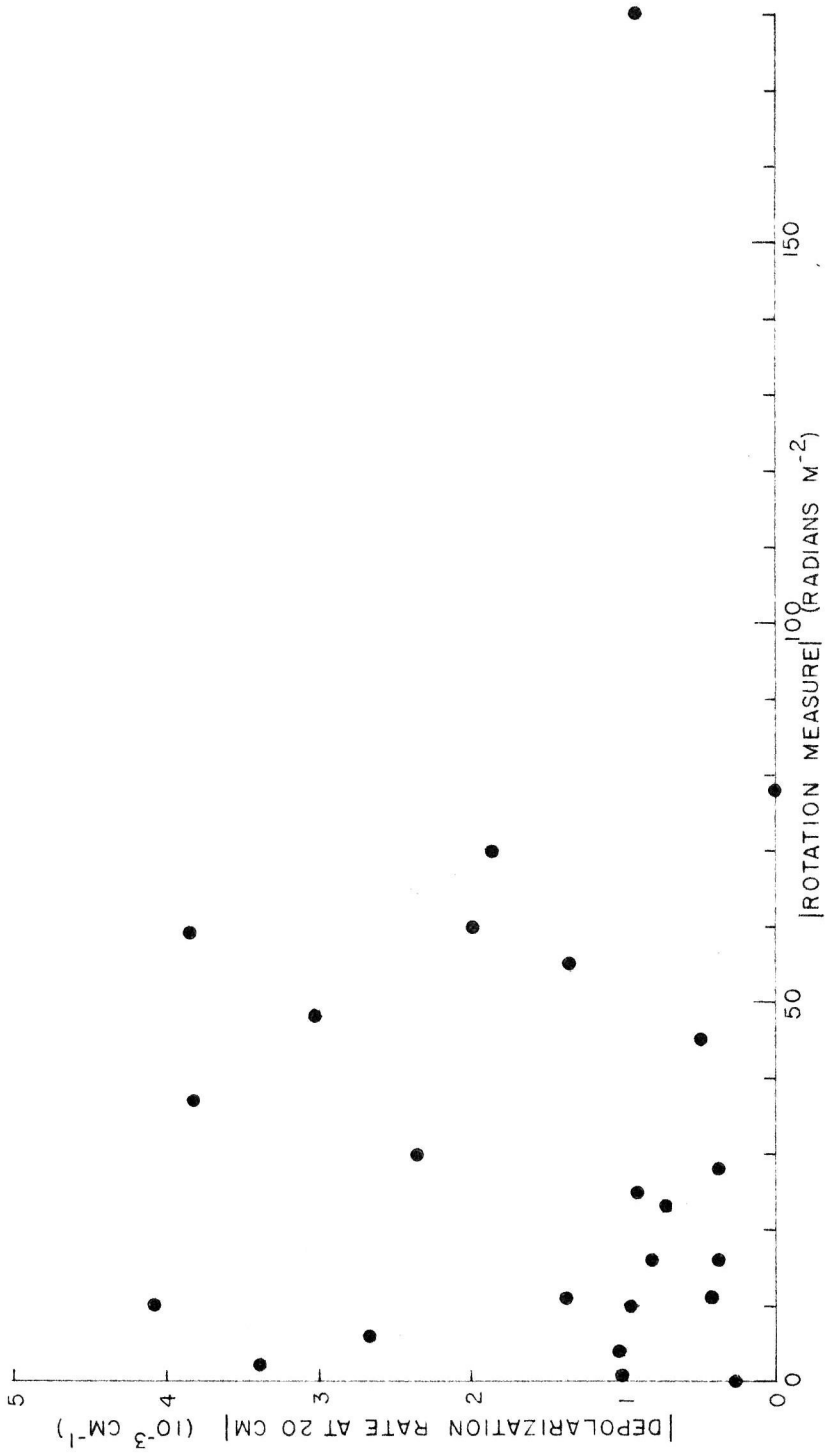

Figure 18. Plot of |depolarization rate at 20 cm| vs. |rotation measure|.

We conclude that the rate of depolarization at 20 cm is probably not influenced by properties of the Galaxy.

The observed depolarization could possibly occur in the intergalactic medium. However, radiation from 3C-48 travels through this medium for a distance of 1100 megaparsecs and still exhibits polarization. Polarized radiation is also received from 3C-273 and Hercules A, whose distances are nearly 500 megaparsecs.

A more likely hypothesis is that the depolarization occurs within the emitting source itself. This has been suggested for the Crab Nebula by several investigators (4), (8), (10), (11), (15), (23). Woltjer (34) has hypothesized that a magneto-ionic medium exists in extragalactic radio sources, and that this is the origin of their depolarization.

A homogeneous magneto-ionic medium either within or surrounding the source would produce an effective depolarization via the Faraday effect (23). However, this mechanism cannot account for the sources which have positive depolarization rates. Furthermore, Faraday rotation would occur at the source itself, and the galactic effects mentioned in the preceding section would be much less prominent.

A model in which the magnetic field and/or the ionized-gas distribution have a complicated and irregular structure, and in which emission and rotation occur together, could account for depolarization rates of both signs with little net Faraday rotation. This model has been proposed by Gardner and Whiteoak (13), who believe that, according to

this picture, sources with high brightness temperatures should have large negative depolarization rates; objects with low surface brightnesses should have small depolarization rates. Such is not the case, as can be seen by examining Figure 19 where the depolarization rate at 20 cm is plotted as a function of the brightness temperature at that wavelength. Outstanding exceptions are 3C-227 and 3C-286, the former source having a low brightness temperature and a large depolarization rate and the latter a high brightness temperature and a small depolarization rate. Figure 19 illustrates that depolarization rate and brightness temperature have no apparent relationship.

It is possible that the Faraday effect is not the depolarizing agent. This effect is strongly frequency-dependent, while in general the degree of polarization does not change very rapidly with frequency, especially below 3000 Mc/s.

The observed depolarization could be caused by a change in the source dimensions with wavelength. There is evidence that the polarized radiation comes from a smaller region than the unpolarized (see Chapter IV). If as the wavelength of observation increases more radiation is received from the less polarized outer regions, the degree of polarization would decrease. This frequency-dependent change in dimensions has been observed in the Crab Nebula (35), as well as in some core-halo objects.

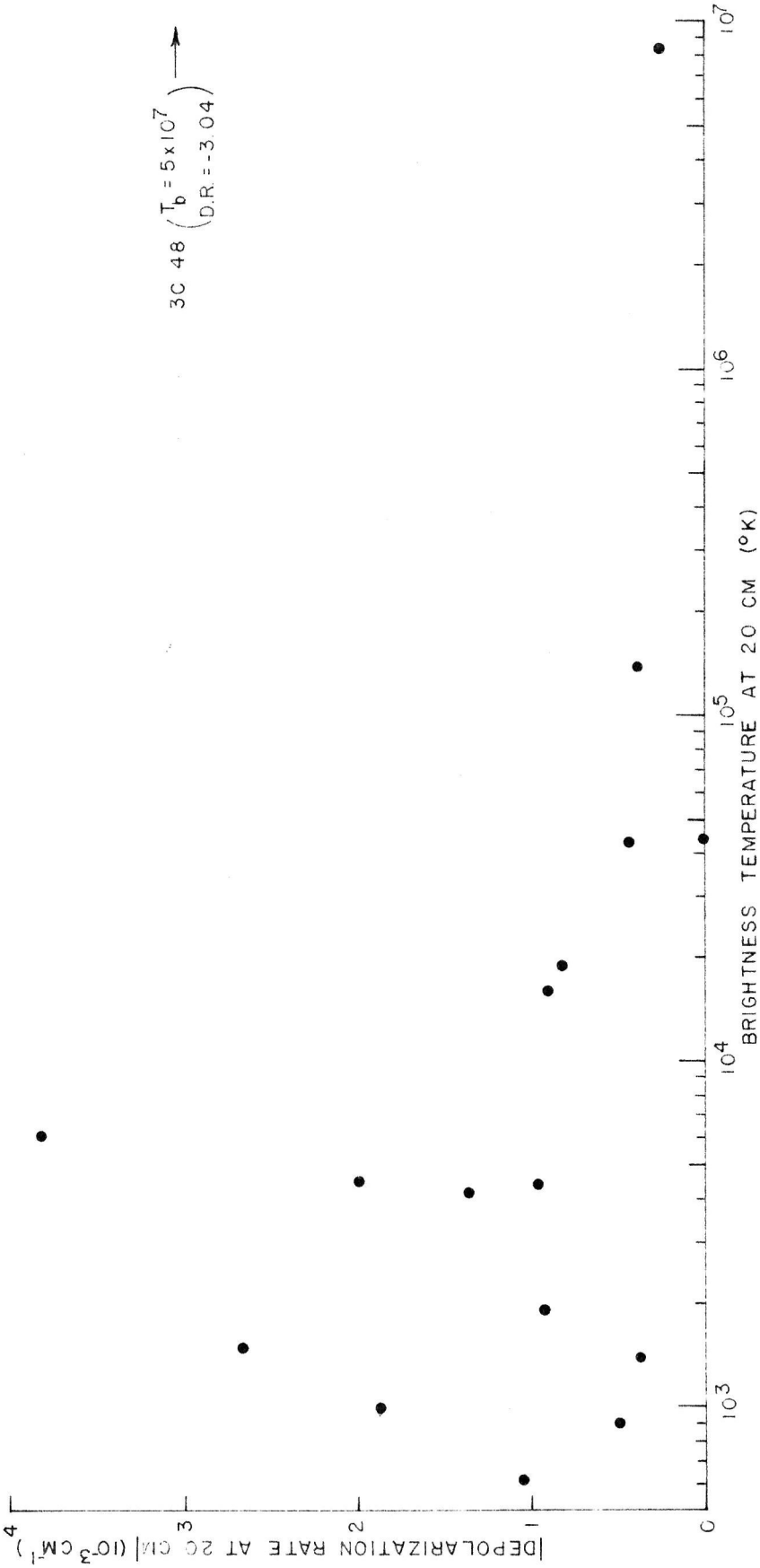

Figure 19. Plot of |depolarization rate at 20 cm| vs. brightness temperature at 20 cm.

Although it appears likely that the change in polarization with frequency is effected in the emitting source, a unique depolarizing mechanism cannot be determined from present measurements. Observations at higher frequencies would be desirable.

Further Comments

Table 5 contains information concerning the intrinsic polarization angle for those sources known to be double. The fourth column in this table lists the smaller angle between the major axis and the plane of polarization. For the twelve double sources listed, this angle is between 0° and 30° for three sources, between 30° and 60° for three, and between 60° and 90° for six. Thus, the magnetic field associated with a double source appears to have no unique structure, contrary to a suggestion by Gardner and Whiteoak (13). These authors noted a tendency for the double sources to fall into two classes: one in which the plane of polarization is roughly parallel to the major axis, and another in which it is roughly perpendicular. More will be said about the double sources in Chapter IV.

Davies and Verschuur (16) have studied the dependence of the degree of polarization on various physical properties of the radio sources. At a wavelength of 21 cm they detected no correlation with spectral index, nor with brightness temperature, nor with redshift. Their data agreed poorly with other published results, and their measurements are

Table 5. Features of the Double Sources

Source	P.A. of Major Axis, A	Intrinsic Pol. Angle, P	|P-A|
3C-33	$20^\circ \pm 8^\circ$	$101^\circ \pm 6^\circ$	$81^\circ \pm 10^\circ$
Fornax A(a)	100	66	34
Fornax A(b)		103	3
3C-98	25 ±10	66 ±10	41 ±14
3C-111	60 ± 7	160 ±20	80 ±21
Pictor A	90	110	20
3C-227	90 ±10	159 ±12	69 ±16
3C-270	85 ± 7	105	20
3C-273	45	141 ±10	84
Centaurus A(a)	46.5± 2	147	80
3C-327	90	145 ± 5	55
Hercules A	100.5±1.5	21 ± 7	86 ± 7
Cygnus A	109 ±1.5	166 ±10	57 ±10

being repeated. Their conclusions, however, are not altered by the present data at any frequency. It should be pointed out that the degree of polarization at decimeter wavelengths may be as much a property of any intervening depolarizing medium as of the emitting source itself.

An interesting correlation has been found. Figure 20 is a plot of the percentage polarization at 2840 Mc/s as a function of the logarithm of the magnetic field in the emitting source. The procedure for calculating these fields has been described by Maltby, Matthews, and Moffet (31). It involves minimizing the source's total energy, the sum of its relativistic particle and magnetic field energies. The underlying assumptions have been described by Burbidge (36).

There is a definite trend for the polarization fraction at 2840 Mc/s to decrease as the magnetic field increases. Only the source 3C-78 disrupts the pattern. A possible interpretation is that the depolarizing mechanism operating in radio sources is more effective for those having strong magnetic fields. The source Cygnus A, for example, which has a relatively strong field of 2×10^{-4} oersteds, changes from a percentage polarization of 7.5 per cent at 3.15 cm to only 0.5 per cent at 9.45 cm. The depolarization rate at 20 cm, however, seems to be independent of magnetic field strength (see Figure 21). Additional observations at high frequencies ($\sim$3cm) of sources having strong fields would help resolve this question.

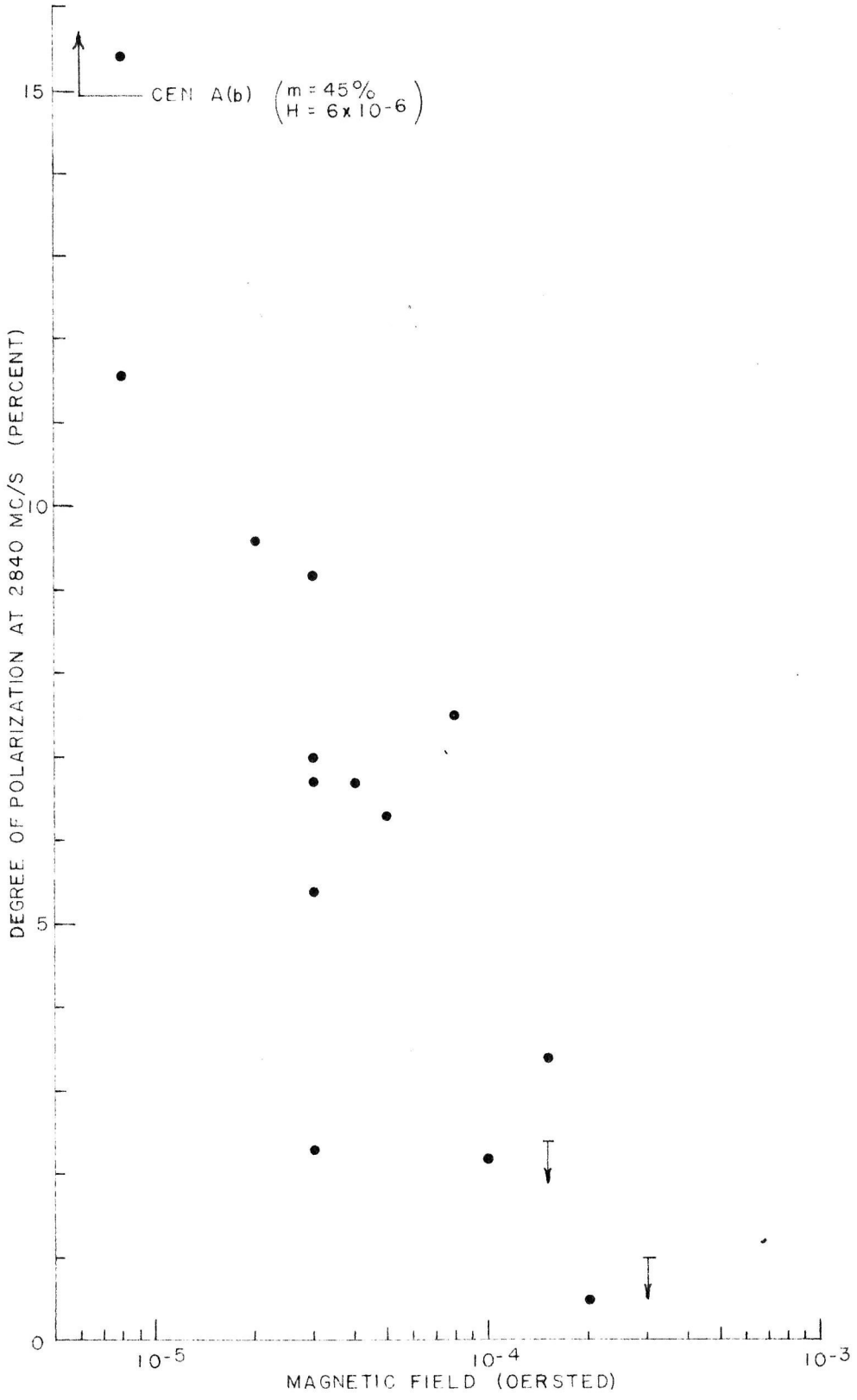

Figure 20. Dependence of observed degree of polarization at 2840 Mc/s on magnetic field within the emitting source. The symbol ↓ indicates an upper limit.

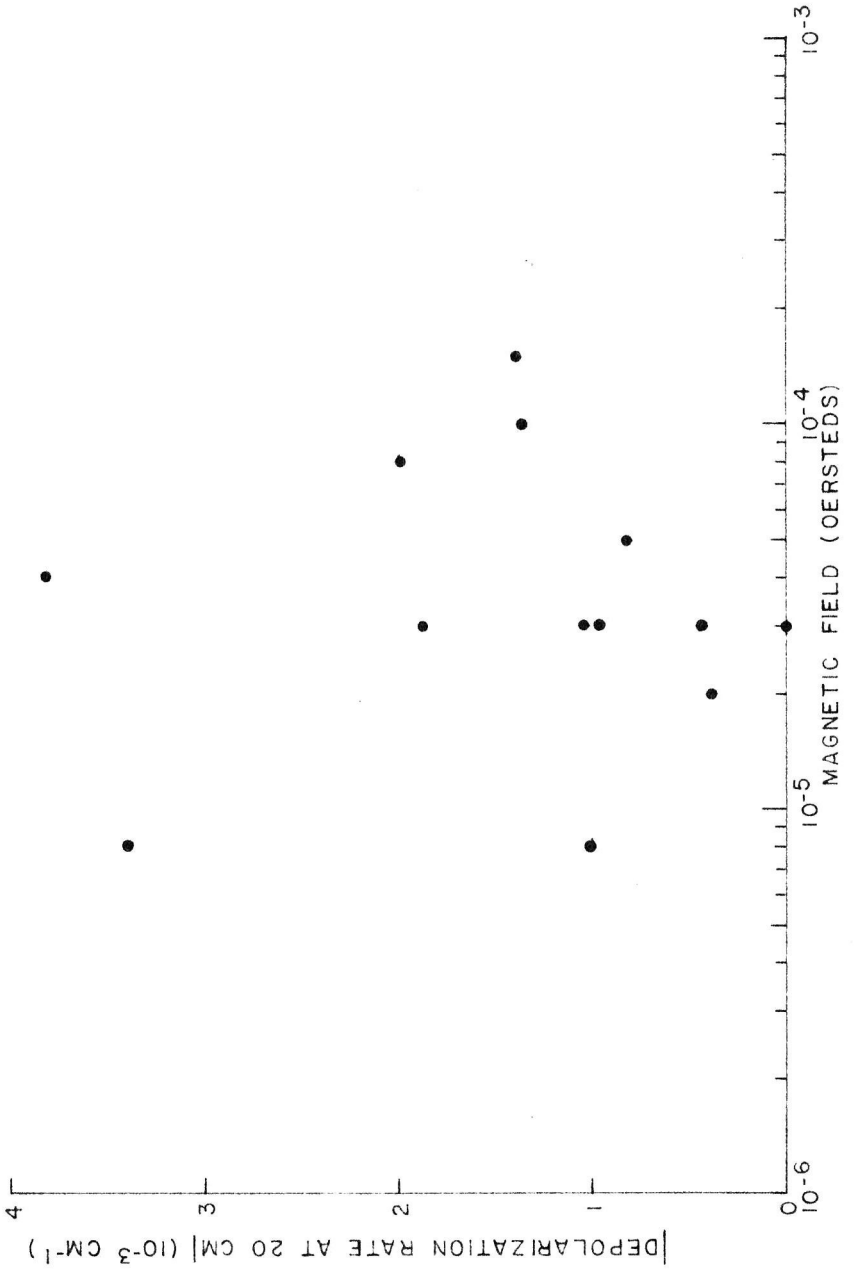

Figure 21. Plot of | depolarization rate at 20 cm | vs. magnetic field within the emitting source.

CHAPTER IV

Observational Technique and Results for Resolved Sources

When the source dimensions are not small relative to the fringe period $1/s$ of the interferometer, the approximations used in Chapter II are no longer valid. Assuming linearly polarized feed horns aligned along the directions 1 and 2, the interferometer response to these partially resolved sources is given by

$$R_{12}(t) = G\{V_{12}(s_x,s_y)\cos[\Phi_{12}(s_x,s_y)-2\pi s_x\Omega\, t+\Psi] - \Gamma_{12}(s_x,s_y)\sin[\sigma_{12}(s_x,s_y)-2\pi s_x\Omega\, t+\Psi]\}\ , \tag{7}$$

with the complex Fourier transforms defined by

$$V_{12}(s_x,s_y)e^{i\Phi_{12}(s_x,s_y)} = \int\int A(x,y)C_{12}(x,y)e^{i2\pi(s_xx+s_yy)}dx\ dy, \tag{8}$$

$$\Gamma_{12}(s_x,s_y)e^{i\sigma_{12}(s_x,s_y)} = \int\int A(x,y)S_{12}(s,y)e^{i2\pi(s_xx+s_yy)}dx\ dy. \tag{9}$$

Consider the coordinate systems shown in Figure 22. ξ and η are orthogonal axes, as are Υ and ϵ. The $\xi\eta$-system is inclined at 45° to the $\Upsilon\epsilon$-system. A partially polarized electromagnetic wave is propagating into the paper along a normal to the two coordinate systems. The state of this wave is completely specified by the four quantities I, m, r, and χ. Here I represents the total intensity, that is the sum of the polarized component I_p and the unpolarized

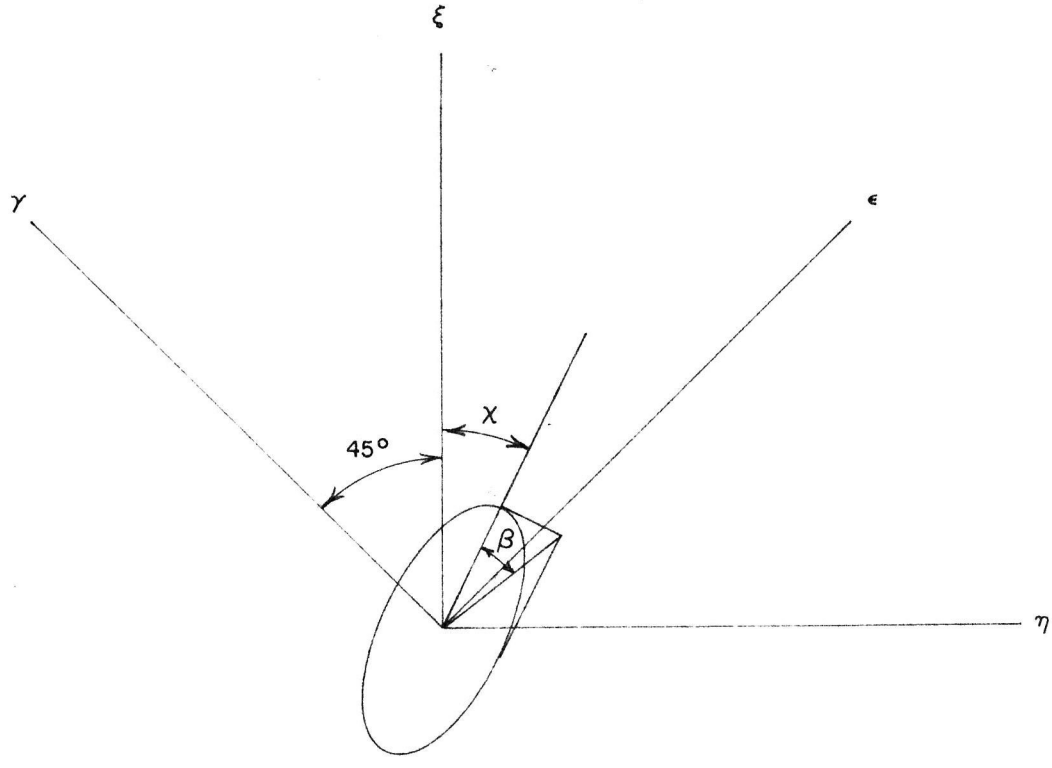

Figure 22. Cartesian coordinate systems inclined at 45° to each other. An elliptically polarized electromagnetic wave is propagating alongan axis perpendicular to the plane of the paper. The polarization ellipse is inclined at an angle χ , and its axial ratio is tan β .

component I_u; m is the polarization fraction, defined as the ratio I_p/I; r is the axial ratio of the polarization ellipse; χ is the position angle of its major axis.

Cohen (23) has emphasized that for radio astronomical polarization measurements the state of the wave is more conveniently specified by the four Stokes parameters I, Q, U, and V. The advantage of this representation is that the Stokes parameters are closely related to actual antenna measurements. In fact, with reference to the $\xi\eta$-coordinate system, the quantities C and S defined by equations (5) and (6) bear the following relations to the Stokes parameters(37):

$$C_{\xi\xi}(x,y) = \langle E_\xi^2(x,y)\rangle \equiv I_\xi \quad , \tag{36}$$

$$C_{\eta\eta}(x,y) = \langle E_\eta^2(x,y)\rangle \equiv I_\eta \quad , \tag{37}$$

$$C_{\xi\eta}(x,y) = \langle E_\xi(x,y)E_\eta(x,y)\cos\left[\psi_\xi(x,y)-\psi_\eta(x,y)\right]\rangle \equiv \frac{1}{2}U \quad , \tag{38}$$

$$S_{\xi\eta}(x,y) = \langle E_\xi(x,y)E_\eta(x,y)\sin\left[\psi_\xi(x,y)-\psi_\eta(x,y)\right]\rangle \equiv \frac{1}{2}V \quad . \tag{39}$$

The parameters I and Q are determined from

$$I \equiv I_\xi + I_\eta \tag{40}$$

and

$$Q \equiv I_\xi - I_\eta \quad . \tag{41}$$

Cohen (23) has pointed out that rotation of the coordinate axes through 45° interchanges Q and (-U). Hence,

in the $\gamma\epsilon$-system, we have

$$C_{\gamma\gamma}(x,y) = I_{\gamma} \quad , \tag{42}$$

$$C_{\epsilon\epsilon}(x,y) = I_{\epsilon} \quad , \tag{43}$$

$$C_{\gamma\epsilon}(x,y) = (1/2)\,Q \quad , \tag{44}$$

$$S_{\gamma\epsilon}(x,y) = (1/2)\,V \quad , \tag{45}$$

and

$$I = I_{\gamma}+I_{\epsilon} \quad , \tag{46}$$

$$U = I_{\epsilon}-I_{\gamma} \quad . \tag{47}$$

Thus, a knowledge of the values of C determined with orthogonal feed horns at two positions separated by 45°, of S with orthogonal feeds at one of these positions, and of C with both feeds parallel to one of these four axes permits determination of all four Stokes parameters.

The Stokes parameters are related to the usual properties specifying partially polarized radiation by the equations

$$I = I \quad , \tag{48}$$

$$Q = I_p \cos 2\beta \cos 2\chi \quad , \tag{49}$$

$$U = I_p \cos 2\beta \sin 2\chi \quad , \tag{50}$$

$$V = I_p \sin 2\beta \quad , \tag{51}$$

where

$$\beta = \tan^{-1} r \quad . \tag{52}$$

The equivalence of these relations with those used in equations (36) through (41) is demonstrated by Chandrasekhar (37). Obviously,

$$m = (Q^2+U^2+ V^2)^{1/2}/ I \quad , \tag{53}$$

$$\tan 2\beta = V/(Q^2+U^2)^{1/2} \quad , \tag{54}$$

$$\tan 2\chi = U/Q \quad . \tag{55}$$

The quantities C and S are not directly measurable. Instead, the Fourier transforms of these quantities are determined from the observations. From equation (7) it is apparent that a single observation with one feed horn, say A, in position angle p_1 and the other, B, in p_2 will not suffice to determine both transforms. It is also necessary to observe with feed A in angle p_2 and feed B in angle $(p_1+180°)$. If the phase advance in the first configuration of the signal in A over the signal in B is $(\psi_1-\psi_2)$, then in the second configuration it is $\left[\pi-(\psi_1-\psi_2)\right]$. If we denote the first configuration by the subscripts 12 and the second by 2(-1), then

$$C_{12}(x,y) = -C_{2(-1)}(x,y) \tag{56}$$

and

$$S_{12}(x,y) = S_{2(-1)}(x,y). \tag{57}$$

Consequently,

$$V_{12}(s_x,s_y) = V_{2(-1)}(s_x,s_y) \quad , \tag{58}$$

$$\Phi_{12}(s_x,s_y) = \Phi_{2(-1)}(s_x,s_y)-\pi \quad , \tag{59}$$

and

$$\Gamma_{12}(s_x,s_y) = \Gamma_{2(-1)}(s_x,s_y) \quad , \tag{60}$$

$$\sigma_{12}(s_x,s_y) = \sigma_{2(-1)}(s_x,s_y) \quad . \tag{61}$$

The interferometer response in the second configuration is thus

$$R_{2(-1)}(t) = G\{-V_{12}(s_x,s_y)\cos[\Phi_{12}(s_x,s_y)-2\pi s_x \Omega t+\Psi] - \Gamma_{12}(s_x,s_y)\sin[\sigma_{12}(s_x,s_y)-2\pi s_x \Omega t+\Psi]\} \quad . \tag{62}$$

It follows that

$$1/2[R_{12}(t)-R_{2(-1)}(t)]=GV_{12}(s_x,s_y)\cos[\Phi_{12}(s_x,s_y)-2\pi s_x\Omega t+\Psi], \tag{63}$$

$$-1/2[R_{12}(t)+R_{2(-1)}(t)]=G\Gamma_{12}(s_x,s_y)\sin[\sigma_{12}(s_x,s_y)-2\pi s_x\Omega t+\Psi], \tag{64}$$

The form of equations (63) and (64) is identical to that obtained for the interferometer response to a discrete source when the feed horns are assumed parallel. The method of obtaining visibility amplitudes and phases from equations of this type has been described by Moffet (20).

Maltby and Moffet (38) have discussed the problem of extracting the source brightness distribution from a complex Fourier transform. In the present analysis the transformed quantities are the Stokes parameters characterizing the radiation, and it is their distribution over the source which is sought. The same methods of interpretation, namely Fourier inversion and model fitting, are applicable in principle. Because of the introduction of several new parameters characterizing the polarized portion of the radiation, however, the complexity of fitting a model visibility function to the observed one is greatly enhanced. The number of free parameters has increased sufficiently that very detailed observational data are required to distinguish between different models. Furthermore, since the polarized radiation is only a few per cent of the total, accurate measurements of points on the visibility curves are more difficult to obtain. These difficulties will be apparent when the individual sources are discussed.

One-Dimensional Distribution

Heretofore most interferometric observations have been made with only a single baseline orientation. This is also the case here, where an east-west baseline has been used. In such a case, if the observations are made near meridian transit, the value of s_y is zero and s_x is equal to s. The visibility functions become

$$V_{12}(s,0)e^{i\Phi_{12}(s,0)} = \iint A(x,y)C_{12}(x,y)e^{i2\pi sx}dx\ dy \qquad (65)$$

and

$$\Gamma_{12}(s,0)e^{i\sigma_{12}(s,0)} = \iint A(x,y)S_{12}(x,y)e^{i2\pi sx}dx\ dy. \qquad (66)$$

Let the one-dimensional distributions of C_{12} and S_{12} be defined by

$$A(x)C_{12}(x) = \int A(x,y)C_{12}(x,y)dy, \qquad (67)$$

$$A(x)S_{12}(x) = \int A(x,y)S_{12}(x,y)dy\ . \qquad (68)$$

If the one-dimensional visibility functions are

$$V_{12}(s)e^{i\Phi_{12}(s)} \equiv V_{12}(s,0)e^{i\Phi_{12}(s,0)} \qquad (69)$$

and

$$\Gamma_{12}(s)e^{i\sigma_{12}(s)} = \Gamma_{12}(s,0)e^{i\sigma_{12}(s,0)}\ , \qquad (70)$$

then equations (65) and (66) become

$$V_{12}(s)e^{i\Phi_{12}(s)} = \int A(x)C_{12}(x)e^{i2\pi sx}dx \qquad (71)$$

and

$$\Gamma_{12}(s)e^{i\sigma_{12}(s)} = \int A(x)S_{12}(x)e^{i2\pi sx}dx \qquad (72)$$

With reference to the $\xi\eta$- and $\Upsilon\varepsilon$-coordinate systems (see Figure 22), these visibility functions are complex Fourier transforms of the various Stokes parameters weighted by the antenna power response A(x). According to equations (36), (38), (39), and (44), we have

$$V_{\xi\xi}(s)e^{i\Phi_{\xi\xi}(s)} = \mathcal{F}\left[A(x)I_{\xi}(x)\right]\ , \qquad (73)$$

$$V_{\gamma\varepsilon}(s)e^{i\Phi_{\gamma\varepsilon}(s)} = (1/2)\mathcal{F}\left[A(x)Q(x)\right] , \tag{74}$$

$$V_{\xi\eta}(s)e^{i\Phi_{\xi\eta}(s)} = (1/2)\mathcal{F}\left[A(x)U(x)\right] , \tag{75}$$

$$\Gamma_{\xi\eta}(s)e^{i\sigma_{\xi\eta}(s)} = (1/2)\mathcal{F}\left[A(x)V(x)\right] . \tag{76}$$

These visibility functions are related to the observed quantity, the interferometer response, through the equations

$$R_{\xi\xi}(t) = GV_{\xi\xi}(s)\cos\left[\Phi_{\xi\xi}(s)-2\pi s\,\Omega\,t+\Psi\right] , \tag{77}$$

$$1/2\left[R_{\gamma\varepsilon}(t)-R_{\varepsilon(-\gamma)}(t)\right] = GV_{\gamma\varepsilon}(s)\cos\left[\Phi_{\gamma\varepsilon}(s)-2\pi s\,\Omega\,t+\Psi\right] , \tag{78}$$

$$1/2\left[R_{\xi\eta}(t)+R_{\eta(-\xi)}(t)\right] = +GV_{\xi\eta}(s)\cos\left[\Phi_{\xi\eta}(s)-2\pi s\,\Omega\,t+\Psi\right], \tag{79}$$

$$1/2\left[R_{\xi\eta}(t)+R_{\eta(-\xi)}(t)\right] = -G\Gamma_{\xi\eta}(s)\sin\left[\sigma_{\xi\eta}(s)-2\pi s\,\Omega\,t+\Psi\right]. \tag{80}$$

In summary, the visibility functions are determined directly from the observations in a manner described by equations (77) through (80). The parameters I_ξ, Q, U, and V are extracted from these visibility functions either by Fourier inversion, as prescribed by equations (73) through (76) or by model fitting. The Stokes parameter I is obtained from the relation

$$I = 2I_\xi - Q . \tag{81}$$

The orientation angle χ and the axial ratio r of the polarization ellipse, and the polarization fraction m, are determined from the Stokes parameters, using equations (52)

through (55).

Linearly Polarized Radiation

If synchrotron radiation emitted by ultrarelativistic charged particles in a magnetic field is the radiating mechanism in the observed radio sources, then we expect the polarization of these sources to be very nearly linear. Korchakov and Syrovat-skii (4) have shown that the Stokes parameter V for radiation emitted by a system of particles in a constant uniform magnetic field, the particle distribution being isotropic with respect to both spatial coordinates and direction of motion, is zero. According to equation (54), this implies that the polarization is linear. For an anisotropic distribution of particles V is proportional to mc^2/E, which for ultrarelativistic particles is extremely small. Hence the assumption of linear polarization is well justified.

For linearly polarized radiation the phase difference between any two components is either 0° or 180°. In either case the sine of the phase difference, and therefore S_{12}, is zero. Thus, only the visibility function $V_{12}e^{i\Phi 12}$ need be considered.

The one-dimensional distributions over the source of the three remaining non-zero Stokes parameters, I, Q, and U, can be recovered from the complex visibility functions obtained with only three feed-horn configurations: one in which the feeds are parallel to a given axis; a second in

which one feed is parallel and the other perpendicular to this axis; and a third configuration of orthogonal feeds inclined at 45° to the two axes defined above. This statement is expressed symbolically in equations (73) through (75).

Fewer measurements are required to determine these visibility functions, since the vanishing of S_{12} means that $R_{12}(t)=-R_{2(-1)}(t)$. As a result, we have simply

$$R_{\xi\xi}(t) = GV_{\xi\xi}(s)\cos\left[\Phi_{\xi\xi}(s)-2\pi s\,\Omega\, t+\Psi\right] , \qquad (77)$$

$$R_{\gamma\epsilon}(t) = GV_{\gamma\epsilon}(s)\cos\left[\Phi_{\gamma\epsilon}(s)-2\pi s\,\Omega\, t+\Psi\right] , \qquad (82)$$

$$R_{\xi\eta}(t) = GV_{\xi\eta}(s)\cos\left[\Phi_{\xi\eta}(s)-2\pi s\,\Omega\, t+\Psi\right] . \qquad (83)$$

The instrumental parameters G and Ψ are obtained from observations of suitably chosen calibration sources. The method has been discussed by Moffet (20).

The expressions relating the polarization fraction and the position angle of the plane of polarization to the Stokes parameters simplify to

$$m = (Q^2+U^2)^{1/2}/I \qquad (84)$$

and

$$\tan 2\chi = U/Q \qquad (85)$$

in the case of linearly polarized radiation.

Model Fitting

In the Appendix we have calculated the visibility functions corresponding to the Fourier transforms of Q and U for some simple assumed model sources. It was found con-

venient to orient the $\xi\eta$- and $\gamma\epsilon$-coordinate systems by requiring that $V_{\xi\eta}(s)e^{i\Phi_{\xi\eta}(s)}$, the Fourier transform of $U(\mathbf{x})$, be zero at zero antenna separation. Thus, the ξ-axis has been aligned parallel to the plane of polarization as determined by a single-antenna measurement.

In addition, it was shown that the visibility amplitude $V_{\gamma\epsilon}$, when evaluated at zero separation, was half the single-antenna flux of the polarized radiation; it therefore makes a convenient normalizing factor for the visibility amplitudes. Consequently, we introduced new visibility amplitudes $V_<(s)$ and $V_\llcorner(s)$, which are, respectively, $V_{\gamma\epsilon}(s)$ and $V_{\xi\eta}(s)$ divided by $V_{\gamma\epsilon}(0)$. The corresponding phases, $\Phi_<(s)$ and $\Phi_\llcorner(s)$, remain unchanged, and are simply $\Phi_{\gamma\epsilon}(s)$ and $\Phi_{\xi\eta}(s)$, respectively (see equations 89 through 92 in the Appendix).

An examination of the model visibility functions calculated in the Appendix reveals that the single-source models are readily handled. If it is assumed that the position angle of the plane of polarization is the same throughout the emitting region, then by virtue of our choice of coordinate axes the visibility amplitude $V_\llcorner(s)$ will be zero at all antenna separations. The only free parameter is the source diameter. For a given model it will therefore be possible to plot two families of curves representing the visibility amplitude $V_<(s)$ and the phase $\Phi_<(s)$, each member of a family differing only in the value of the source diameter. The curves which most closely fit the observed

data can then be accepted as defining the distribution of polarized radiation within the source.

Unfortunately, sources with two or more distinct regions of emission cannot be handled so easily. In the most general type of double source the free parameters are the source separation, the relative intensities of the two components, the individual diameters, and the individual polarization angles. With so many quantities to be varied it is no longer feasible to plot families of model curves; multi-dimensional model surfaces would now be required. It is more reasonable to seek clues from the observed data suggesting a particular type of model, and to then select the set of parameters describing the best fit with the aid of a computer.

The very real danger exists that unless detailed observational data are available the model accepted as defining the best fit might be a poor approximation to the actual source. For example, a model double source having equal-diameter but unequal-intensity components might easily be fitted to a few observed points obtained from an actual source consisting of two unequal-diameter and equal-intensity components. Because of the increased number of parameters needed to specify polarized radiation, this danger is greater than for the case of model fitting to unpolarized sources. It should also be pointed out that, because the polarized radiation comprises only a few per cent of the

total, large percentage errors exist in the measured points on the visibility curves. This increases the difficulty of selecting a realistic model.

Comments on Individual Sources

A preliminary attempt at determining the distribution of polarized radiation has been made for a few sources. The purpose of this preliminary investigation was more to develop the technique of observation and analysis than to obtain detailed information about the sources observed. As a result, only limited data are available, consisting of measurements of the visibility amplitudes $V_{\swarrow}(s)$ and $V_{\llcorner}(s)$ at at most four antenna separations. No phase measurements have been made.

Nevertheless, it was considered worthwhile to attempt to fit a model to a few of the sources studied. It must be emphasized that because of the scarcity of data, the chosen models may not accurately represent the actual source distributions. They are included only to indicate the kinds of information to be expected from an analysis of this type.

The data are presented individually for each source. The frequency is given in megacycles/second. Fluxes are listed in units of $10^{-26}\mathrm{Wm}^{-2}(\mathrm{c/s})^{-1}$. The quoted errors are estimates of the standard deviation. Unless otherwise noted, the data on the unpolarized radiation were those of Maltby and Moffet (38). The zero-spacing measurements of Cygnus A were provided by Mayer (39). All other single-

antenna measurements were made by Gardner and Whiteoak (13).

A few comments are included to support the particular choice of model. If a double-source model was selected, the component separation was assumed to be the same as for the unpolarized radiation.

Pictor A. The fact that $V_L(s)$ does not remain zero at nonzero values of s means that the orientation angle of the plane of polarization is not constant throughout the emitting region. This fact is consistent with a double-source model, each component of which is polarized at a different angle.

Table 6

Features of the Polarized Radiation in Pictor A

	Frequency	Polarized Flux	Spacing		
			0	290λ	340λ
	2840	1.14±0.21			
$V_L(s)$			0.0±0.09	1.40±0.14	
$V_<(s)$			0.92±0.23	0.39±0.07	
	1666	3.76±0.80			
$V_L(s)$			0.0 ±0.17		1.19±0.08
$V_<(s)$			0.83±0.21		0.78±0.13
	1420	3.94±0.80			
$V_L(s)$			0.0 ±0.10	0.53±0.10	
$V_<(s)$			0.90±0.20	1.09±0.10	

We shall further assume that the model type does not change with frequency. Then the fact that at a frequency of 1420 Mc/s $V_<(290\lambda)$ is greater than $V_<(0)$ eliminates any model having equal-intensity components. As the next simplest case we try a model with equal-diameter components.

Figure 23 shows how the observations are fitted by a double-Gaussian model with an east-west separation of 4'.6, each component having a diameter of 1'.5. These properties are assumed to be independent of frequency. The smaller of the angles between the planes of polarization of the two sources is taken to be 60° at all frequencies. The assumption that this angle does not change with frequency is supported by the observation that the Faraday rotation of polarized radiation occurs in the Galaxy (see Chapter III). The ratio of intensities of the two components is 1.2:1 at 2840 Mc/s, 1.7:1 at 1666 Mc/s, and 3.5:1 at 1420 Mc/s. The absence of phase measurements makes it impossible to determine which component is the stronger, or even whether the same component is stronger at all frequencies.

The unpolarized components have equal intensities at 960 Mc/s. If they are assumed equal at all other frequencies as well, then the polarization fractions for the two components are 3.8 per cent and 4.5 per cent at 2840 Mc/s, 2.3 per cent and 3.9 per cent at 1666 Mc/s, and 1.4 per cent and 4.8 per cent at 1420 Mc/s. The 1'.5-diameter for the polarized radiation is less than the diameter of 2' occupied by the unpolarized radiation. Thus, the degree of polarization in the central region of each source is greater than the figures quoted above.

There is an ambiguity in the values of the polarization angles of the two sources which can only be resolved

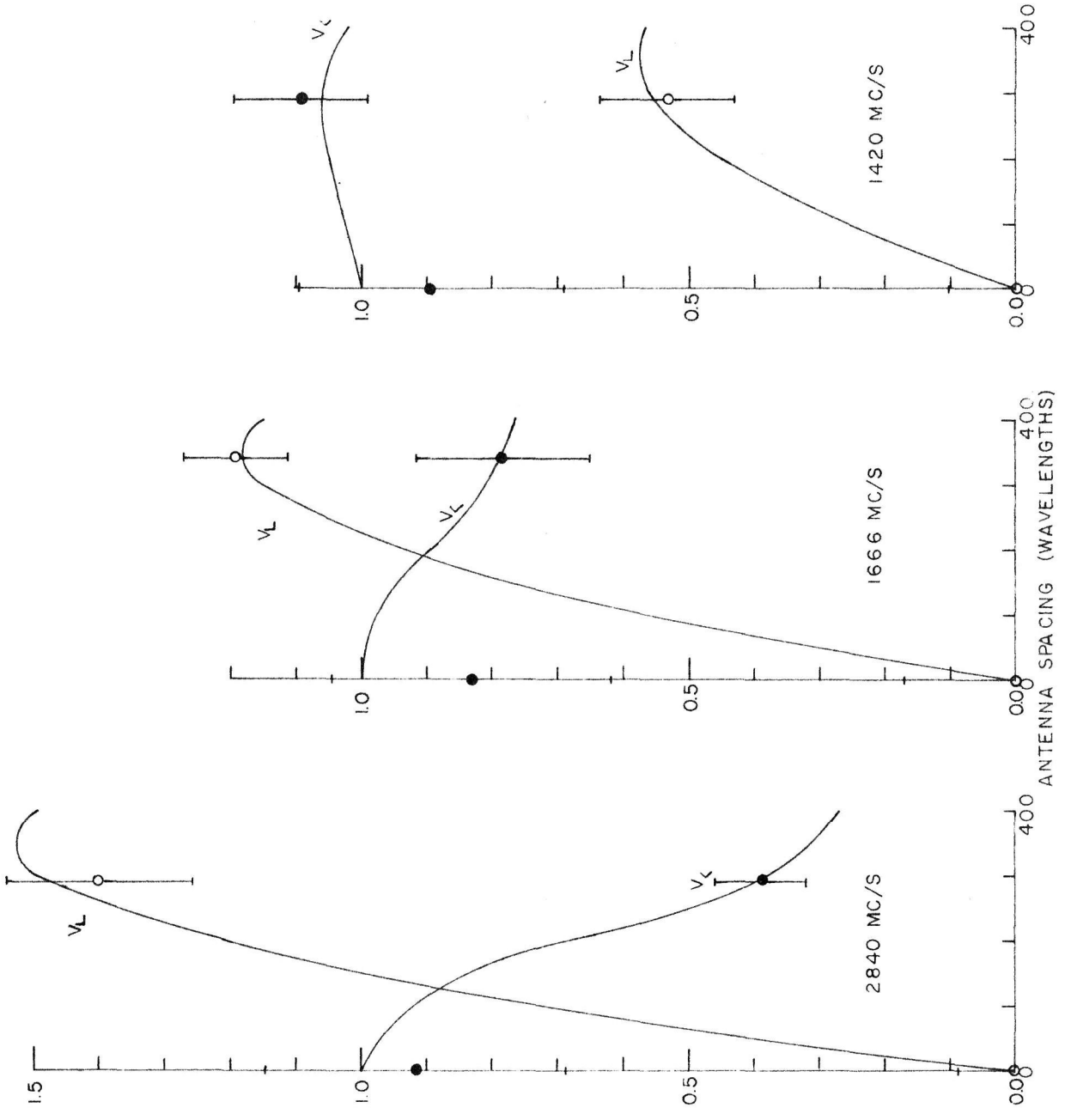

Figure 23. Model fit for Pictor A. See text for details.

by a knowledge of phases. The two possibilities at each frequency are summarized in Table 7, which also includes an extrapolation to infinite frequency to eliminate effects of Faraday rotation. This extrapolation is made on the assumption that the same component is the stronger at all frequencies.

Table 7

Polarization Angles for the Two Components of Pictor A

	Frequency			
	2840	1666	1420	∞
Stronger Source	143° 91°	32° 176°	58° 42°	122° 52°
Weaker Source	83° 151°	152° 56°	178° 102°	62° 112°

Crab Nebula. $V_{\perp}(s)$ remains very near to zero at all spacings, indicating that the polarization angle is constant throughout the region of emission. The observational points are fitted very well by a single-Gaussian model whose diameter to half-brightness is 1'.8, as can be seen by referring to Figure 24. For this source alone, the data is sufficient to justify a measure of confidence in the accuracy of the model.

Table 8

Features of the Polarized Radiation in the Crab Nebula

Freq.		Polarized Flux	Spacing 0	578λ	1100λ	1250λ
	2840	23.8±1.2				
$V_{\perp}(s)$			0.0±0.08		0.12±0.08	0.06±0.08
$V_{<}(s)$			1.0±0.05	0.72±0.08	0.42±0.09	0.21±0.08

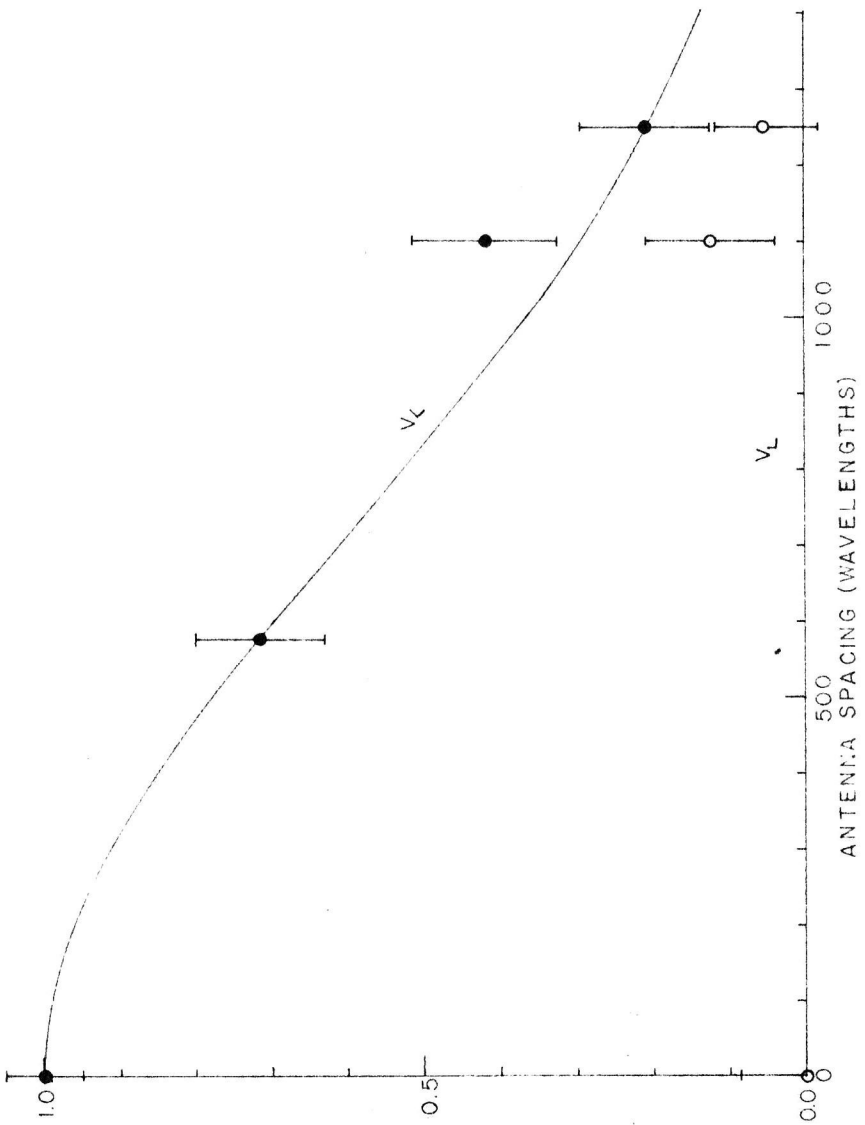

Figure 24. Model fit for Crab Nebula. See text for details.

The polarized radiation is confined to a smaller region than the unpolarized, whose diameter in position angle 90° is 3'.3. An estimate of the average percentage polarization within a diameter of 1'.8 can be made by assuming the unpolarized radiation has a Gaussian distribution. This is an excellent assumption in the case of the Crab Nebula (20). A simple integration shows that 47 per cent of the unpolarized radiation lies within a radius of 0'.9. Since the average polarization fraction including all the unpolarized radiation is 3.9 per cent, it is approximately 3.9/0.47=8.3 per cent within the central 0'.9 of the source. The polarization angle in this region is 132°. Within this same region the optical radiation is polarized to the extent of approximately 16 per cent in position angle 160°(8).

The fact that the polarized radiation exhibits more central concentration than the unpolarized radiation could be explained by a random orientation of the magnetic field at large radii. Optical measurements by Oort and Walraven (8) seem to confirm this hypothesis. Furthermore, ionized gas is known to be present in the filaments (33). Therefore, it is possible that a polarized electromagnetic wave propagating from the central region suffers Faraday rotations of many different magnitudes and senses before leaving the source. This mechanism could account for the observed decrease in degree of polarization between optical frequencies

and 10 cm.

Centaurus A (Central Component)

Again the departure of $V_L(s)$ from zero eliminates any simple single-source model. The data at 2840 Mc/s indicate that $V_L(s)$ periodically returns to zero. Thus, an equal-diameter model suggests itself.

Figure 25 illustrates how the observed data are fitted by a model source consisting of two 1'.3-diameter components separated in an east-west direction by 5'. The discrepancy at 1290λ is not considered serious since it occurs near a minimum, where the two major components have largely canceled each other and a small irregularity can produce pronounced effects. The E-vectors of the polarized radiation are inclined at 44° to each other. As in the case of Pictor A, these properties are assumed to be independent of frequency. The ratios of polarized fluxes for the two components are 4.5:1 at 2840 Mc/s, 7.1:1 at 1666 Mc/s, and 7.7:1 at 1420 Mc/s.

The lack of phase measurements again prevents identification of the stronger polarized component from this data alone. It also makes it impossible to distinguish between the possible pairs of polarization position angles presented in Table 10.

Table 9

Features of the Polarized Radiation in Centaurus A

	Freq.	Polarized Flux	Spacing				
			0	290λ	340λ	580λ	1290λ
	2840	11.2±2.2					
$V_L(s)$			0.0 ±0.09	0.42±0.05		0.17±0.09	0.32±0.06
$V_<(s)$			0.82±0.20	0.87±0.10		0.83±0.09	0.34±0.02
	1666	14.9±4.0					
$V_L(s)$			0.0 ±0.27		0.25±0.18		
$V_<(s)$			1.22±0.26		0.91±0.17		
	1420	17.0±6.0					
$V_L(s)$			0.0 ±0.12	0.21±0.12			
$V_<(s)$			1.32±0.35	0.96±0.12			

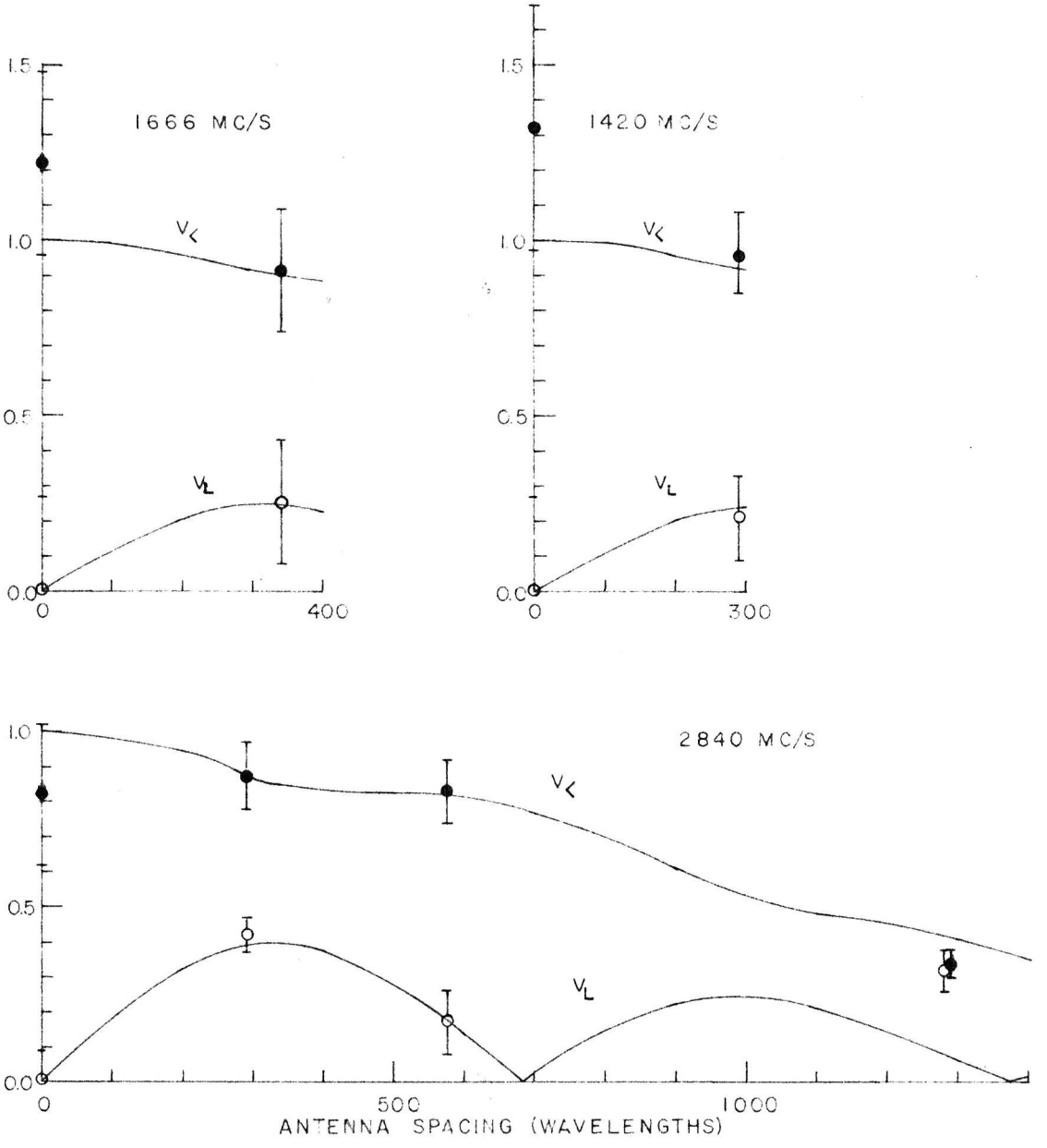

Figure 25. Model fit for central component of Centaurus A. See text for details.

Table 10

Polarization Angles
for the Two Components of Centaurus A

	Frequency			
	2840	1666	1420	∞
Stronger Source	121° 109°	41° 33°	179° 171°	158° 146°
Weaker Source	77° 153°	177° 77°	135° 35°	114° 10°

Bracewell, Cooper, and Cousins (25) have shown that at 3000 Mc/s the northeast component of the central source in Centaurus A is polarized 15 per cent in position angle 115°. These values change to 9 per cent in 40° at 1650 Mc/s and 7 per cent in 175° at 1410 Mc/s (26). Polarization in the southwest component has not previously been detected.

Cooper and Price (26) find by extrapolating to infinite frequency that the intrinsic polarization angle of northeast component is 147°. If we identify our stronger component with the northeast source, then the second pair of polarization angles in Table 10 should be used at all frequencies (for example, 33° and 77° at 1666 Mc/s).

If we again assume that our stronger source of polarized radiation is in the northeast, we can calculate the polarization fraction of the southwest component. Bracewell, Cooper, and Cousins (25) find the ratio at 3000 Mc/s of northeast to southwest unpolarized fluxes to be 78:66=1.2:1. This value is in agreement with that at 960 Mc/s (38). If we adopt this ratio for all frequencies,

then the southwest source is polarized to the extent of 4.5 per cent at 2840 Mc/s, 1.6 per cent at 1666 Mc/s, and 1.2 per cent at 1420 Mc/s.

It is worth noting that the east-west diameter of the polarized regions, namely 1!3, is significantly smaller than the 2!4 overall diameters of the individual sources.

Hercules A

The points at 1245λ violate all of the simple models discussed in the Appendix. Additional data are required before a more complex model is attempted.

Table 11

Features of the Polarized Radiation in Hercules A

	Freq.	Polarized Flux	Spacing			
			0	290λ	575λ	1245λ
	2840	1.38±0.12				
$V_L(s)$			0.0±0.08		0.29±0.14	1.09±0.22
$V_<(s)$			1.00±0.09	0.86±0.08	0.72±0.14	1.19±0.20

3C-353

Once again the visibility amplitude $V_L(s)$ rises from zero, indicating that there is more than one region of constant polarization angle. An equal-diameter, double-Gaussian model can be fitted to the observations, as is shown in Figure 26.

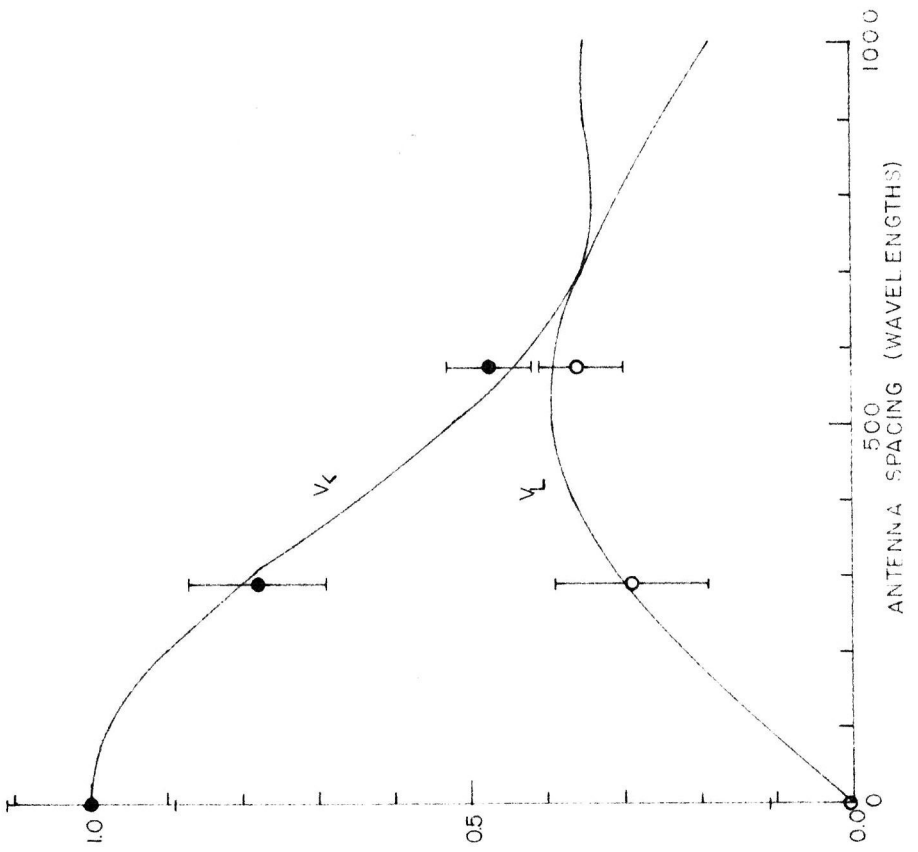

Figure 26. Model fit for 3C-353. See text for details.

Table 12

Features of the Polarized Radiation in 3C-353

	Freq.	Polarized Flux	Spacing		
			0	290λ	575λ
	2840	1.8±0.2			
V_L (s)			0.0+0.11	0.29+0.10	0.36+0.06
$V_<$ (s)			1.00±0.11	0.78±0.09	0.47±0.06

The common diameters are taken to be 1.'6, and the east-west component separation is 2.'5. The ratio of the fluxes of polarized radiation are 2.3:1. The E-vector of the stronger component is in position angle 114° or 96°. The corresponding position angles for the weaker component are 81° and 129°. If the relative fluxes are assumed independent of frequency, the effects of Faraday rotation can be removed by using the observed rotation measure. The intrinsic polarization angles will then be either 93° and 60° or 75° and 108°, where the position angle of the stronger source has been listed first.

The unpolarized radiation comes from two components with relative intensities of 2:1 and equal diameters of 1.'4±0.'2. Thus, according to our model the polarized radiation occupies at least as large a region as the unpolarized. The polarization fractions of the two components are either approximately equal, or one is about four times the other.

Cygnus A

The polarized radiation cannot come from a single region

within which the polarization angle is constant, or the value of V_L would be zero at s=1290λ. An equal-diameter, equal-intensity, double-source model with any non-imaginary diameter cannot be fitted to the data unless the separation of the polarized components differs from that of the unpolarized.

Table 8

Features of the Polarized Radiation in Cygnus A

	Freq.	Polarized Flux	Spacing	
			0	1290λ
	3200	3.16±1.16		
$V_L(s)$			0.0±0.17	1.26±0.06
$V_{\swarrow}(s)$			1.00±0.37	0.63±0.06

As the most reasonable guess until more detailed data are available, we can assign the diameters of the unpolarized sources to the polarized ones. Thus, we assume sources of 0!7 diameters separated in an east-west direction by 1!59 (40). If the polarized fluxes are in the ratio 1.4:1, and if 63° is the angle between the planes of polarization, the calculated visibility amplitudes fit the observed data as shown in Figure 27. The polarization angle of the stronger source is either 12° or 148°, while the corresponding angles for the weaker component are 129° and 31°. These pairs of angles extrapolated to infinite frequency, assuming a constant ratio of fluxes, become 6° and 123° or 142° and 25°, with the polarization angle of the stronger source appearing first.

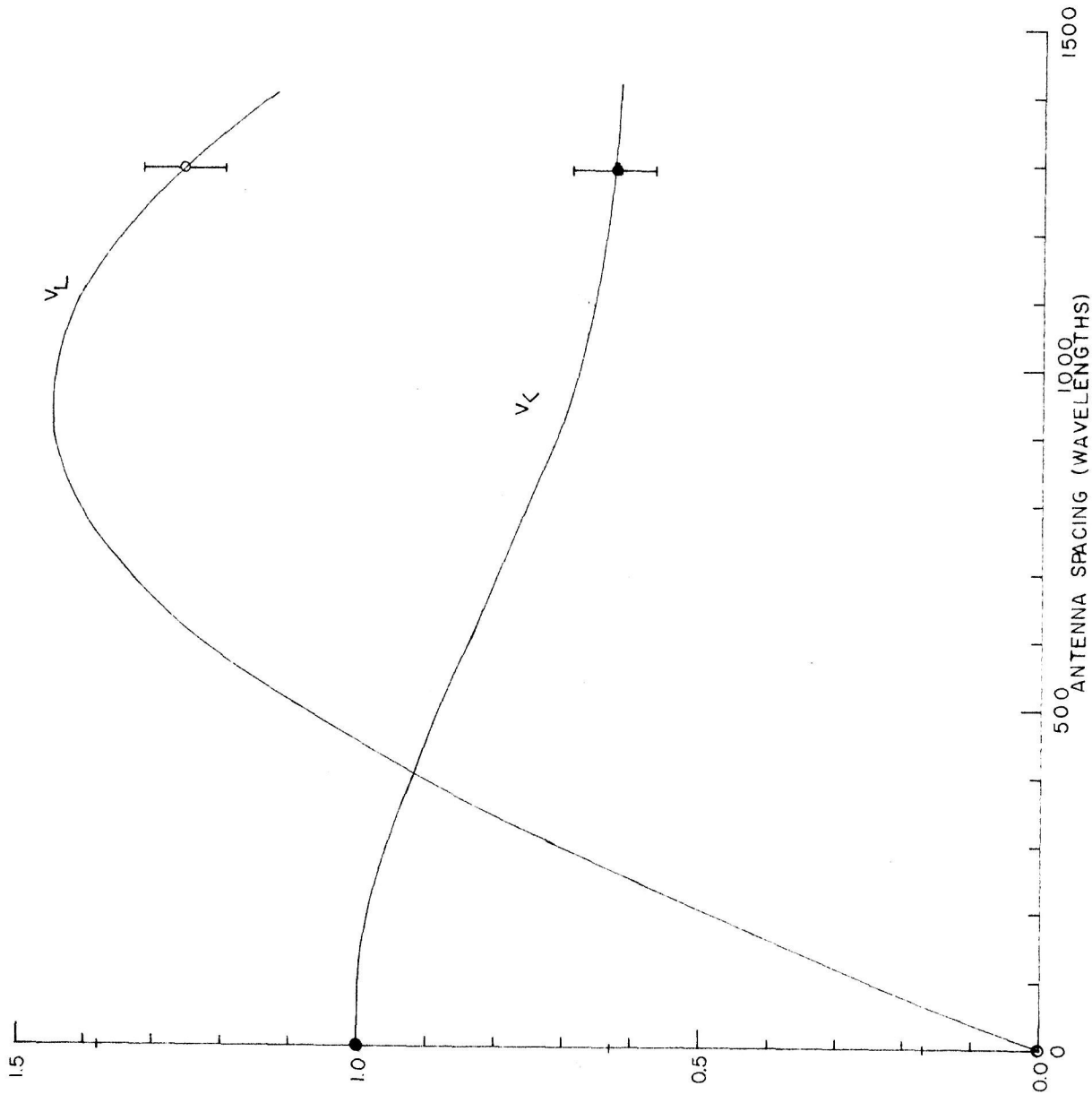

Figure 27. Model fit for Cygnus A. See text for details.

General Conclusions

Although many additional observations are needed before the preceding models can be regarded as realistic, a few general conclusions can be stated. The position angle of the polarized radiation is, in general, different for each of the components of a double source. Furthermore, this difference is not a constant quantity. The orientation of the planes of polarization apparently bears no unique relationship to the major axis. Table 14 contains the position angles of the major axis, the polarization angles of the stronger and weaker components, and the difference between these angles for a few double sources. Where an ambiguity in polarization angle exists both possibilities have been tabulated. The data on Fornax A are taken from Gardner and Whiteoak (13).

Table 14

Intrinsic Polarization Angles for Double Sources

Source	P. A. of Major Axis A	Stronger Source S	Weaker Source W	S-A	W-A
Fornax A	100°	66°	103°	-34°	3°
Pictor A	90°	122°	62°	32°	-28°
		52°	112°	-38°	22°
Centaurus A	46°	146°	10°	100°	-36°
Cygnus A	109°	6°	123°	-103°	14°
		42°	25°	33°	-84°

There is a slight suggestion that the polarized radiation comes from a region of smaller dimensions than the

unpolarized radiation. This could be interpreted as meaning that the magnetic field is relatively uniform over the central region of emission, but becomes more randomly oriented in the periphery.

Finally, it appears that the rates of depolarization differ for the two components of double sources. This could indicate a greater uniformity of magnetic field within one of the sources and/or a disparity in the amounts of ionized gas present.

APPENDIX

Model Sources

We calculate here the visibility functions expected for some simple assumed model sources. We regard these sources as linearly polarized, and consider only transit observations made with the interferometer aligned along an east-west baseline. Under these circumstances the visibility functions of interest are

$$V_{\gamma\epsilon}(s)e^{i\Phi_{\gamma\epsilon}(s)} = \frac{1}{2}\int A(x)Q(x)e^{i2\pi sx}dx$$

$$= \frac{1}{2}\int A(x)Q(x)(\cos 2\pi sx + i\sin 2\pi s_x)\ dx \qquad (74)$$

and

$$V_{\xi\eta}(s)e^{i\Phi_{\xi\eta}(s)} = \frac{1}{2}\int A(x)U(x)e^{i2\pi sx}dx$$

$$= \frac{1}{2}\int A(x)U(x)(\cos 2\pi sx + i\sin 2\pi sx)\ dx. \qquad (75)$$

The $\gamma\epsilon$- and $\xi\eta$-systems are Cartesian systems inclined at 45° to each other, and both are normal to the direction of propagation of the wave (see Figure 22). We do not consider here the visibility function $V_{\xi\xi}(s)e^{i\Phi_{\xi\xi}(s)}$, since in most cases the polarization fraction m is sufficiently small that $I_{\xi}\approx I/2$, independent of the orientation of the ξ-axis. Thus, the visibility functions already published (20), (41), (42) can for most sources be considered Fourier transforms of $A(x)I(x)/2$.

In the case of linearly polarized radiation the necessary Stokes parameters are

$$Q(x) = I_p(x)\cos 2\chi(x) \tag{86}$$

and

$$U(x) = I_p(x)\sin 2\chi(x). \tag{87}$$

To orient the $\xi\eta$- and $\gamma\epsilon$-coordinate systems we arbitrarily specify that the transform of $U(x)$ vanish at zero antenna separation, that is $V_{\xi\eta}(0)=0$. This choice is equivalent to aligning one of the axes, say the ξ-axis, parallel to the plane of polarization as determined by a measurement with a single antenna. Once this orientation has been selected it must, of course, be maintained at all antenna spacings.

With the above choice of axes, the total flux of polarized radiation as measured with a single antenna will be

$$I_p = \int A(x)Q(x)dx = \int A(x)I_p(x)\cos 2\chi(x)dx = 2V_{\gamma\epsilon}(0). \tag{88}$$

It is seen that $V_{\gamma\epsilon}(0)$ makes a convenient normalizing factor for the visibility amplitudes. Accordingly, we introduce the following definitions:

$$V_<(s) = V_{\gamma\epsilon}(s)/V_{\gamma\epsilon}(0)\ , \tag{89}$$

$$V_\perp(s) = V_{\xi\eta}(s)/V_{\gamma\epsilon}(0), \tag{90}$$

$$\Phi_{<}(s) = \Phi_{\gamma\epsilon}(s) \ , \tag{91}$$

$$\Phi_{\perp}(s) = \Phi_{\xi\eta}(s) \ . \tag{92}$$

Thus, the quantities we shall evaluate for the chosen models are

$$V_{<}(s)e^{i\Phi_{<}(s)} = \frac{\int A(x)I_p(x)\cos 2\chi(x)\ (\cos 2\pi sx + i\sin 2\pi sx)dx}{\int A(x)I_p(x)\cos 2\chi(x)dx} \tag{93}$$

and

$$V_{\perp}(s)e^{i\Phi_{\perp}(s)} = \frac{\int A(x)I_p(x)\sin 2\chi(x)\ (\cos 2\pi sx + i\sin 2\pi sx)dx}{\int A(x)I_p(x)\cos 2\chi(x)dx} \ . \tag{94}$$

Circular Gaussian Model

Consider a source whose polarized radiation has a radial distribution which is Gaussian. If its diameter to half-brightness is d_p , then

$$I_p(x) = I_o e^{-x^2/\sigma_p{}^2} \ , \tag{95}$$

where $\sigma_p = 0.61 d_p$. Assume that the plane of polarization has the same position angle everywhere within the emitting region. According to the method by which we have oriented our coordinate systems, the constant value of χ will be zero. Hence

$$V_{\perp}(s) = 0 \ , \qquad \Phi_{\perp}(s) = 0 \tag{96}$$

and

$$V_<(s)e^{i\Phi_<(s)} = \frac{\int A(x)I_p(x)\ (\cos 2\pi sx + i\sin 2\pi sx)dx}{\int A(x)I_p(x)dx} \quad . \tag{97}$$

Equations 96 and 97 are valid for any distribution in which the polarization angle χ is independent of location in the source.

To a reasonable approximation the power response pattern of the antenna can be considered Gaussian. If the antenna beamwidth to half-power is d_a, corresponding to a dispersion $\sigma_a = 0.6 1 d_a$, then we take

$$A(x) = Ae^{-x^2/\sigma_a{}^2} \quad . \tag{98}$$

Since $A(x)I_p(x)$ is an even function, the Fourier sine transform vanishes. The cosine transform is

$$V_<(s)e^{i\Phi_<(s)} = \frac{\int_0^\infty e^{-x^2\left(\frac{1}{\sigma_a{}^2} + \frac{1}{\sigma_p{}^2}\right)} \cos 2\pi sx\ dx}{\int_0^\infty e^{-x^2\left(\frac{1}{\sigma_a{}^2} + \frac{1}{\sigma_p{}^2}\right)} dx} \quad ,$$

or

$$V_<(s) = e^{-(\pi s\sigma_p)^2 / \left(1 + \frac{\sigma_p{}^2}{\sigma_a{}^2}\right)} \quad , \qquad \Phi_<(s) = 0 \quad . \tag{99}$$

The visibility amplitude of equation 99 is a Gaussian. Families of such curves for various diameters have been plotted by Moffet (43).

The beamwidth d_a is directly proportional to the wavelength. At $\lambda = 10.6$ cm the 90-foot paraboloids have a beamwidth of 16'.2, corresponding to a dispersion of

$\sigma_a = 9'.9 = 0.0029$ radians. The beamwidth correction was significant only for diameters of 4' and greater. To avoid including this correction in other models, we restrict the range of diameters to 4' or less.

Uniformly Bright Disk

We again assume that the plane of polarization has the same orientation throughout the emitting region. The transform of U(x) is therefore zero. Let the two-dimensional distribution of polarized radiation be defined by

$$I_p(x,y) = \begin{cases} I_o & \text{for} \quad (x^2+y^2) \leq r^2 \\ 0 & \text{for} \quad (x^2+y^2) > r^2 \end{cases} \tag{100}$$

The corresponding one-dimensional distribution will be

$$I_p(x) = \begin{cases} \int_{-\sqrt{r^2-x^2}}^{\sqrt{r^2-x^2}} I_o dy = 2I_o\sqrt{r^2-x^2} & \text{for} \quad |x| \leq r \\ 0 & \text{for} \quad |x| > r \end{cases} \tag{101}$$

Because $I_p(x)$ is an even function, the sine transform again vanishes. We are left with

$$V_<(s) = \frac{\int_0^r \sqrt{r^2-x^2}\, \cos 2\pi sx\, dx}{\int_0^r \sqrt{r^2-x^2}\, dx} = \frac{(r/4s)J_1(2\pi sr)}{\pi r^2/4} = \frac{J_1(2\pi sr)}{\pi sr}, \tag{102}$$

$$\Phi_<(s) = 0 \quad .$$

This visibility amplitude has also been plotted by Moffet (43) for sources of various diameters.

Double Source Models

Consider a source consisting of two distinct regions of emission. Let the centroid of source 1 be located at x_1 and of source 2 at x_2. The distribution of polarized radiation in source i (i=1,2) is denoted by $I_{pi}(x-x_i)$, and its plane of polarization is in position angle χ_i. The visibility functions can then be written

$$\begin{aligned} V_<(s)e^{i\Phi_<(s)} = &\Big[\cos 2\chi_1 \int I_{p1}(x-x_1)d(x-x_1) \\ &+\cos 2\chi_2 \int I_{p2}(x-x_2)d(x-x_2)\Big]^{-1} \\ &\Big[e^{i2\pi s x_1}\cos 2\chi_1 \int I_{p1}(x-x_1)e^{i2\pi s(x-x_1)}d(x-x_1) \\ &+e^{i2\pi s x_2}\cos 2\chi_2 \int I_{p2}(x-x_2)e^{i2\pi s(x-x_2)}d(x-x_2)\Big] \end{aligned} \tag{103}$$

and

$$\begin{aligned} V_\perp(s)e^{i\Phi_\perp(s)} = &\Big[\cos 2\chi_1 \int I_{p1}(x-x_1)d(x-x_1) \\ &+\cos 2\chi_2 \int I_{p2}(x-x_2)d(x-x_2)\Big]^{-1} \\ &\Big[e^{i2\pi s x_1}\sin 2\chi_1 \int I_{p1}(x-x_1)e^{i2\pi s(x-x_1)}d(x-x_1) \\ &+e^{i2\pi s x_2}\sin 2\chi_2 \int I_{p2}(x-x_2)e^{i2\pi s(x-x_2)}d(x-x_2)\Big] . \end{aligned} \tag{104}$$

Recalling the definition of $V_< e^{i\Phi_<}$ for a single source, first introduced in equation 97, we can express the above equations in the form

$$V_{<}(s)e^{i\Phi_{<}(s)}=(I_{p1}\cos 2\chi_1+I_{p2}\cos 2\chi_2)^{-1}$$

$$\left[e^{i2\pi sx_1}I_{p1}\cos 2\chi_1\ V_{1<}(s)e^{i\Phi_{1<}(s)}\right. \tag{105}$$

$$\left.+e^{i2\pi sx_2}I_{p2}\cos 2\chi_2\ V_{2<}(s)e^{i\Phi_{2<}(s)}\right],$$

$$V_{\llcorner}(s)e^{i\Phi_{\llcorner}(s)}=(I_{p1}\cos 2\chi_1+I_{p2}\cos 2\chi_2)^{-1}$$

$$\left[e^{i2\pi sx_1}I_{p1}\sin 2\chi_1\ V_{1<}(s)e^{i\Phi_{1<}(s)}\right. \tag{106}$$

$$\left.+e^{i2\pi sx_2}I_{p2}\sin 2\chi_2\ V_{2<}(s)e^{i\Phi_{2<}(s)}\right],$$

where the polarized flux for the i-th source has been defined by

$$I_{pi} = \int I_{pi}(x-x_i)d(x-x_i), \qquad i = 1,2. \tag{107}$$

For convenience, we specify that the centroid of polarized emission be at x=0. This requirement is satisfied if

$$x_i = -\frac{I_{p2}}{I_{p1}+I_{p2}}\ X \qquad \text{and} \qquad x_2 = \frac{I_{p1}}{I_{p1}+I_{p2}}\ X\ , \tag{108}$$

where X is the separation between the two sources.

To satisfy the condition that $V_{\llcorner}$ vanish at zero antenna separation we must have

$$-\frac{\sin 2\chi_1}{\sin 2\chi_2} = \frac{I_{p2}}{I_{p1}}\ . \tag{109}$$

With the help of equations 108 and 109, the visibility functions for a double source become

$$V_{<}(s)e^{i\Phi_{<}(s)}=(\cot 2\chi_1-\cot 2\chi_2)^{-1}$$
$$\left[e^{i2\pi sX\sin 2\chi_1(\sin 2\chi_1-\sin 2\chi_2)^{-1}}\cot 2\chi_1\ V_{1<}e^{i\Phi_{1<}}\right.$$
$$\left.-e^{i2\pi sX\sin 2\chi_2(\sin 2\chi_2-\sin 2\chi_1)^{-1}}\cot 2\chi_2 V_{2<}e^{i\Phi_{2<}}\right] \qquad (110)$$

and

$$V_{L}(s)e^{i\Phi_{L}(s)}=(\cot 2\chi_1-\cot 2\chi_2)^{-1}$$
$$\left[e^{i2\pi sX\sin 2\chi_1(\sin 2\chi_1-\sin 2\chi_2)^{-1}}\ V_{1<}e^{i\Phi_{1<}}\right.$$
$$\left.-e^{i2\pi sX\sin 2\chi_2(\sin 2\chi_2-\sin 2\chi_1)^{-1}}\ V_{2<}e^{i\Phi_{2<}}\right]. \qquad (111)$$

Double-Gaussian Model

We consider now a source consisting of two circular Gaussians. According to equation 99, the visibility functions for the individual sources are of the form

$$V_{i<}(s) = e^{-(\pi s\sigma_{pi})^2}, \qquad \Phi_{i<}(s)=0, \qquad i=1,2\ . \qquad (112)$$

The result of substituting these relations into equations 110 and 111 is

$$V_{<}(s) = (\cot 2\chi_1-\cot 2\chi_2)^{-1}$$
$$\left[e^{-2(\pi s\sigma_{p1})^2}\cot^2 2\chi_1+e^{-2(\pi s\sigma_{p2})^2}\cot^2 2\chi_2\right.$$
$$\left.-2e^{-(\pi s\sigma_{p1})^2}e^{-(\pi s\sigma_{p2})^2}\cot 2\chi_1\cot 2\chi_2\cos 2\pi sX\right]^{1/2}, \qquad (113)$$

$$\Phi_<(s) = \tan^{-1}\left[\frac{e^{-(\pi s\sigma_{p1})^{-2}}\cot 2\chi_1 + e^{-(\pi s\sigma_{p2})^2}\cot 2\chi_2}{-e^{-(\pi s\sigma_{p1})^2}\cot 2\chi_1 + e^{-(\pi s\sigma_{p2})^2}\cot 2\chi_2}\tan \pi sX\right] + \frac{\sin 2\chi_2 + \sin 2\chi_1}{\sin 2\chi_2 - \sin 2\chi_1}\pi sX \quad , \tag{114}$$

$$V_<(s) = (\cot 2\chi_1 - \cot 2\chi_2)^{-1} \left[e^{-2(\pi s\sigma_{p1})^2} + e^{-2(\pi s\sigma_{p2})^2} - 2e^{-(\pi s\sigma_{p1})^2}e^{-(\pi s\sigma_{p2})^2}\cos 2\pi sX\right]^{1/2} \quad , \tag{115}$$

$$\Phi_<(s) = \tan^{-1}\left[\frac{e^{-(\pi s\sigma_{p1})^2} + e^{-(\pi s\sigma_{p2})^2}}{-e^{-(\pi s\sigma_{p1})^2} + e^{-(\pi s\sigma_{p2})^2}}\tan \pi sX\right] + \frac{\sin 2\chi_2 + \sin 2\chi_1}{\sin 2\chi_2 - \sin 2\chi_1}\pi sX \quad . \tag{116}$$

It would, of course, be desirable to be able to plot a family of curves representing these visibility amplitudes and phases, each member of the family differing in some parameter. This is obviously impossible, however, because of the large number of free parameters involved. Even in the simplest case of equal-diameter and equal-intensity sources two parameters, the diameter and the polarization angle, remain arbitrary. The problem is now more suitable for computer techniques.

We next turn our attention to some simplified models.

Equal Diameters

We assume here that the diameters of the two components are the same. Then $\sigma_{p1}=\sigma_{p2}=\sigma_p$. Equations 113 through 116 simplify to

$$V_<(s) = (\cot 2\chi_1-\cot 2\chi_2)^{-1}\, e^{-(\pi s\sigma_{p2})^2} \\ (\cot^2 2\chi_1+\cot^2\chi_2-2\cot 2\chi_1\cot 2\chi_2\cos 2\pi sX)^{1/2}, \tag{117}$$

$$\Phi_<(s) = \tan^{-1}\left[\frac{\cot 2\chi_1+\cot 2\chi_2}{-\cot 2\chi_1+\cot 2\chi_2}\right]\tan\pi sX \\ + \frac{\sin 2\chi_2+\sin 2\chi_1}{\sin 2\chi_2-\sin 2\chi_1}\,\pi sX \quad , \tag{118}$$

$$V_L(s) = 2(\cot 2\chi_1-\cot 2\chi_2)^{-1}e^{-(\pi s\sigma_p)^2}\sin\pi sX \quad , \tag{119}$$

$$\Phi_L(s) = \frac{\pi}{2} + \frac{\sin 2\chi_2+\sin 2\chi_1}{\sin 2\chi_2-\sin 2\chi_1}\,\pi sX \quad . \tag{120}$$

A distinguishing feature of the equal-diameter model is that $V_L(s)$, the visibility amplitude corresponding to the transform of the Stokes parameter U(x), periodically returns to zero.

Equal Intensities

Consider the case of sources with equal fluxes, but not necessarily equal diameters. If $I_{p1}=I_{p2}$, then by

equation 109

$$\sin 2\chi_1 = -\sin 2\chi_2 \quad ,$$

or

$$\chi_1 = -\chi_2 = \chi \quad . \tag{121}$$

We now have for the visibility amplitudes and phases the expressions

$$V_<(s) = \frac{1}{2}\left[e^{-2(\pi s\sigma_{p1})^2} + e^{-2(\pi s\sigma_{p2})^2} + 2e^{-(\pi s\sigma_{p1})^2} e^{-(\pi s\sigma_{p2})^2} \cos 2\pi sX \right]^{1/2} , \tag{122}$$

$$\Phi_<(s) = \tan^{-1}\left[\frac{-e^{-(\pi s\sigma_{p1})^2} + e^{-(\pi s\sigma_{p2})^2}}{e^{-(\pi s\sigma_{p1})^2} + e^{-(\pi s\sigma_{p2})^2}} \tan \pi sX \right] , \tag{123}$$

and

$$V_\perp(s) = \frac{1}{2} \tan 2\chi \left[e^{-2(\pi s\sigma_{p1})^2} + e^{-2(\pi s\sigma_{p2})^2} - 2e^{-(\pi s\sigma_{p1})^2} e^{-(\pi s\sigma_{p2})^2} \cos 2\pi sX \right]^{1/2} , \tag{124}$$

$$\Phi_\perp(s) = \tan^{-1}\left[\frac{e^{-(\pi s\sigma_{p1})^2} + e^{-(\pi s\sigma_{p2})^2}}{-e^{-(\pi s\sigma_{p1})^2} + e^{-(\pi s\sigma_{p2})^2}} \tan \pi sX \right] . \tag{125}$$

It is noted that in an equal-intensity model $V_<(s)$ for all nonzero values of s is less than $V_<(0)$. This is not necessarily true for a source with unequal intensities.

Equal Intensities and Equal Diameters

If both the intensities and the diameters are equal, the visibility amplitudes and phases assume their simplest forms. In this case

$$V_{<}(s) = e^{-(\pi s \sigma_p)^2} \cos \pi s X \quad , \tag{126}$$

$$\Phi_{<}(s) = 0 \quad , \tag{127}$$

$$V_{\llcorner}(s) = e^{-(\pi s \sigma_p)^2} \tan 2\chi \sin \pi s X \quad , \tag{128}$$

$$\Phi_{\llcorner}(s) = \pi/2 \quad . \tag{129}$$

REFERENCES

1. Alfven, H. and Herlofson, N., Phys. Rev. 78, 616 (1950).

2. Westfold, K. C., Astrophys. J. 130, 241 (1959).

3. LeRoux, E., Ann. d'Astrophys. 24, 71 (1961).

4. Korchakov, A. A. and Syrovat-skii, S. I., Soviet Astron.-AJ 5, 678 (1962).

5. Shkovsky, I. S., Doklady Akad. Nauk S.S.S.R. 90, 983 (1953).

6. Dombrovsky, V. A., Doklady Akad. Nauk S.S.S.R. 94, 1021 (1954).

7. Vashakidze, M. A., Astron. Tsirk. 147, 11 (1954).

8. Oort, J. H. and Walraven, Th., Bull. Astron. Inst. Netherlands 12, 285 (1956).

9. Mayer, C. H., McCullough, T. P., and Sloanaker, R. M., Astrophys. J. 126, 468 (1957).

10. Mayer, C. H., McCullough, T. P., and Sloanaker, R. M., paper presented to the XIIIth General Assembly, U.R.S.I., London, 1960.

11. Kuz'min, A. D. and Udal'tsov, V. A., Soviet Astron.-AJ 5, 850 (1962).

12. Mayer, C. H., McCullough, T. P., and Sloanaker, R. M., Astron. J. 67, 581 (1962).

13. Gardner, F. F. and Whiteoak, J. B., paper presented at the Symposium on the Physics of Nonthermal Radio Sources, N.A.S.A., New York, 1962.

14. Haddock, F. T. and Hobbs, R. W., Astron. J. 68, 75 (1963).

15. Morris, D. and Radhakrishnan, V., Astrophys. J. 137, 147 (1963).

16. Davies, R. D. and Verschuur, G. L., Nature 197, 32 (1963).

17. Ryle, M. and Smith, F. G., Nature 162, 462 (1948).

18. Brown, R. H., Palmer, H. P., and Thompson, A. R., Monthly Notices Roy. Astron. Soc. 115, 487 (1955).

19. Mayer, C. H., McCullough, T. P., and Sloanaker, R. M., Astrophys. J. 135, 656 (1962).

20. Moffet, A. T., Astrophys. J. Suppl. No. 67 (1962).

21. Read, R. B., Trans. Inst. Radio Engrs. AP-9, 31 (1961).

22. Hatanaka, T., Publ. Astron. Soc. Japan 8, 73 (1956).

23. Cohen, M. H., Proc. Inst. Radio Engrs. 46, 172 (1958).

24. Barat, J., Lequeux, J., and LeRoux, E., Compt. rend. 251, 2476 (1960).

25. Bracewell, R. N., Cooper, B. F. C., and Cousins, T. E., Nature 195, 1289 (1962).

26. Cooper, B. F. C. and Price, R. M., Nature 195, 1084 (1962).

27. Gardner, F. F. and Whiteoak, J. B., Phys. Rev. Letters 9, 197 (1962).

28. Rose, W. K., Bologna, J. M., and Sloanaker, R. M., Astron. J. 68, 78 (1963).

29. Browne, I. C., Evans, J. V., Hargreaves, J. K., and Murray, W. A. S., Proc. Phys. Soc. (London) B69, 901 (1956).

30. Kellermann, K. I., private communication (1963).

31. Maltby, P., Matthews, T. A. and Moffet, A. T., Astrophys. J. 137, 153 (1963).

32. Sciama, D. W., Nature 196, 760 (1962).

33. Woltjer, L., Bull. Astron. Inst. Netherlands 14, 39 (1958).

34. Woltjer, L., Astrophys. J. 136, 1152 (1962).

35. Parijsky, Y. N., Izv. Pulkovo Astron. Obs. 21, No. 5, 45 (1960).

36. Burbidge, G. R., Astrophys. J. 123, 178 (1956).

37. Chandrasekhar, S., Radiative Transfer (Oxford University Press, London, England, 1950), pp. 24-35.

38. Maltby, P. and Moffet, A. T., Astrophys. J. Suppl. No. 67 (1962).

39. Mayer, C. H., McCullough, T. P., and Sloanaker, R. M., communicated privately by Mayer (1963).

40. Rowson, B., Monthly Notices Roy. Astron. Soc. 119, 26 (1959).

41. Lequeux, J., Ann. d'Astrophys. 25, 221 (1962).

42. Allen, L. R., Anderson, B., Conway, R. G., Palmer, H. P., Reddish, V. C., and Rowson, B., Monthly Notices Roy. Astron. Soc. 124, 477 (1962).

43. Moffet, A. T., Ph.D. Thesis, California Institute of Technology (1961).